UNIVERSITY OF LATVIA
FACULTY OF PHYSICS AND MATHEMATICS

Varis Karitans

INFLUENCE OF OPTICAL AND NEURAL FACTORS ON QUALITY OF THE PERCEIVED IMAGE

SUMMARY OF DOCTORAL THESIS

Submitted for the Doctoral Degree in Physics
Subfield: Medical Physics

Supervisor: Prof., *Dr. hab. phys.* Maris Ozolins

Riga 2012

The doctoral work was developed in the period from 2007 to 2011 in the Faculty of Physics and Mathematics, Department of Optometry and Vision Science, University of Latvia.

The doctoral work has been supported by European Social Fund.

EIROPAS SOCIĀLAIS FONDS

EIROPAS SAVIENĪBA

LATVIJAS UNIVERSITĀTE
ANNO 1919

IEGULDĪJUMS TAVĀ NĀKOTNĒ

Eiropas Sociālā fonda projekts „Atbalsts doktora studijām Latvijas Universitātē” Nr.2009/0138/ 1DP/1.1.2.1.2./ 09/IPIA/ VIAA/004.

Scientific advisor: Prof., *Dr. habil. phys.* **Maris Ozolins**

Reviewers:

Prof., *Dr. habil. phys.* **Ivars Lacis**, University of Latvia
Prof., *Dr. habil. biol.* **Juris Imants Aivars**, University of Latvia
Dr. **Frank Stein**, Ifa systems AG Frechen/Cologne

Chairperson of the Specialized Promotion Council of the Physics, Astronomy and Mechanics: Prof., *Dr. habil. phys.* **Jānis Spīgulis**

The defense of the doctoral thesis will take place in an open session of the Promotion Council on 23rd april 2012 at 17.00 o'clock in the Faculty of Physics and Mathematics, Zellu street 8, Riga.

The doctoral work is available at the Library of the University of Latvia (Kalpaka boulevard 4), Latvian Academic library (Rupniecibas street 10) andin the Faculty of Physics and Mathematics (room F210).

ISBN 978-9984-45-491-7

Contents

Abstract

An eye is an optical system suffering from optical aberrations. Ocular aberrations influence both visual perception and visibility of retinal features. As technologies of adaptive optics advanced it became possible to control optical quality of an eye at very high level.

Dependence of visual functions on optical quality of an eye is widely studied. There is no scientific agreement regarding the role of ocular aberrations in visual perception. In the work, adaptation to the optical defects of an eye and sensitivity of the visual system to different aberrations has been studied. Color vision experiments confirm the role of adaptation processes in visual perception.

The role of optical quality of an eye in assessing the diameter of retinal blood vessels and in interpretation of the results of ophthalmoscopy has been prooved. Wavefront correctors have been designed and their applicability has been studied. The wavefront correctors designed are suited for calibration of aberrometers.

1. INTRODUCTION

1.1. Significance of the work

Initially, adaptive optics was used in astronomy to correct turbulence effects in atmosphere. Later on vision scientists started to use adaptive optics to control the optical quality of an eye. At the beginning of the studies of visual functions it was assumed that a simple relationship exists between visual performance and the optical quality of an eye, i.e., visual performance increases as the level of optical defects of an eye is reduced. In the doctoral work, attention has been paid to an important question whether the visual system makes use of ocular optical defects, i.e., whether the visual system has adapted to these defects. Nowadays, very popular means of refractive correction are power progressive lenses suffering from many optical defects. When starting to wear the power progressive lenses visual perception is impaired because of distortions of an image and adaptation of the visual system to ocular optical defects determines how long time is required for the subject to get accustomed to wearing the power progressive lenses.

Correction of complex ocular optical defects in advanced ophthalmoscopy methods allows to image details (photoreceptors, capillaries etc.) the size of which is only several microns. In the doctoral work, attention has been paid to the role of aberrations in conventional ophthalmoscopy. Optometrists and ophthalmologists are aware of the role of aberrations when correcting refractive errors whereas when examining the fundus of an eye they often don't take into account the fact that appearance of retinal features is affected by ocular optical defects.

Correction of complex ocular optical defects is possible only in a laboratory. In order to assure high optical quality of an eye in daily life, it is necessary to design correctors of complex optical defects so that these correctors can be used similarly to the traditional corrective means. In the doctoral work it has been analyzed how easily such wavefront correctors can be designed by using basic lithography techniques.

In vision science distribution and the amount of various ocular aberrations in a large population has been widely studied. Discrepancy between measurements done by different authors is often observed. Little literature regarding analysis of this discrepancy is available. In the doctoral work attention has been paid to whether differences in calibration of wavefront sensors can result in differences between aberration measurements as observed when comparing reults obtained by various authors.

1.2. The goal of the work

The main goal of the doctoral work is to investigate the role of optical and neural factors in visual perception, ophthalmology and aberrometry.

In order to achieve the goal of the doctoral work the following tasks were performed:

1. influence of the optical quality of an eye on spatial vision was studied;
2. the largest intraocular difference of aberrations that can be tolerated when designing power progressive lenses was measured;
3. adaptation of the visual system to the chromatic content of a stimulus was studied;
4. influence of ocular aberrations on the diameter of retinal blood vessels was studied;
5. the structure and optical properties of wavefront correctors created in a photoresistive layer was assessed using different methods;
6. the relationship between the measured amount of aberrations and calibration parameters of the adaptive optics system was studied.

1.3. Novelty of the work

In the doctoral work influence of intraocular difference of aberrations on ability of the visual system to fuse two images has been analyzed for the first time. In vision science few studies on how intraocular differences of aberrations influence stereo vision have been carried out. However, no authors have analyzed how ability of the visual system to fuse two images depends on the optical quality of an eye. The results obtained in the doctoral work point to adaptation processes of the binocular visual system not studied previously.

In the doctoral work it has been shown for the first time that different aberration patterns cause significant changes in the apparent diameter of the retinal blood vessels. It has been also shown the changes of the A/V ratio caused by aberrations are comparable to those caused by different retinal and systemic pathologies.

In the doctoral work applicability of a binary grayscale phase mask for creating wavefront correctors was evaluated for the first time using different methods (aberrometry, scanning electron microscopy and profilometry). Although applicability of a binary grayscale phase mask in lithography has been widely studied it hasn't been used for creating wavefront modulators.

1.4. Defended thesis

1. The blur caused by ocular aberrations is used by the visual system to ensure a specific function – Vernier acuity. The visual system interpolates many signals of photoreceptors to locate a line with precision which is higher than the limit imposed by the density of photoreceptors. In the region of low correction level of aberrations Vernier acuity is high because the brain uses a large number of photoreceptors to locate a line and because the optical quality of an eye is similar to its natural optical quality. In the region of a high level of correction

of aberrations Vernier acuity is high because the image on a retina is sharp and has high contrast.

2. In the doctoral dissertation it has been prooved that the visual system is able to adapt to the optical defects of eyes. Throughout the life a human visual system adapts to aberrations which keep steady amount and have simple point spread functions. Distortion of an image is the easiest to notice in the case of trefoil whereas it is the most difficult in the case of spherical aberration. The results obtained can be used when designing power progressive lenses.
3. If saturation of colour of a peripheral stimulus is being matched to that of a central stimulus from the achomatic and the maximally saturated side different values of saturation of the peripheral stimulus at the point of subjective equality are obtained. This is called hysteresis of colour saturation. Temporal dependence of saturation of the peripheral stimulus at the point of subjective equality is exponential. The exponential relationship may point to nonlinear processes in photoreceptors involved in adaptation to colour saturation.
4. Aberration patterns with different structure and amount influence retinal images differently. Ocular aberrations can change the A/V ratio significantly compared to the value when the optical quality of an eye is limited by diffraction only. The changes in the A/V ratio caused by ocular aberrations are comparable to those caused by ocular pathologies. Pathologic changes in the diameter of retinal blood vessels can be missed due to ocular aberrations. An ophthalmologist must take into account the optical quality of the patient's and her/his own ocular aberrations when examining the fundus of an eye.
5. The shape of the wavefront needed to compensate higher-order ocular aberrations can be obtained by illuminating a photoresistive layer through a binary grayscale mask. Using such a type of the mask results in rapidly varying depth of the photoresistive layer and strong light scattering. If wavefront correctors manufactured by using the binary grayscale mask are used for calibration of aberrometers the light scattering isn't very important. If light scattering is reduced the wavefront correctors can be used to neutralize aberration effects in ophthalmoscopy.
6. Shack-Hartmann wavefront sensors must be calibrated either by using an aspheric lens or by using a single-mode fiber the end of which has been placed far from the entrance pupil of the Shack-Hartmann wavefront sensor. The possible reason why there are differences between the amount of aberrations measured by different Shack-Hartmann wavefront sensors is unequal curvature of the wavefront used for calibration.

2. THEORY

2.1. A notion ‘wavefront’

As light propagates through an optical media the light source is surrounded by a wavefront. First, let’s consider a point source of light. If the optical media is homogeneous, i.e., the refractive index is constant in the volume of the media the wavefront is spherical and becomes a plane in infinity. According to the Huygens-Fresnel principle each point on the wavefront acts as a source of secondary wavelets (see Figure 2.1.1.). The envelope of the secondary wavelets with identical phase is the new wavefront.

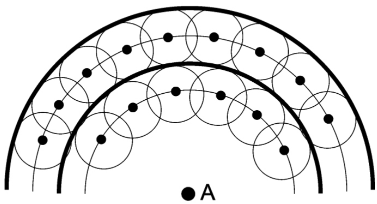

Figure 2.1.1. The Huygens-Fresnel principle for constructing a wavefront. In homogeneous optical media a point light source (A) is surrounded by a spherical wavefront. Each point on the spherical wavefront acts as the secondary source of a wavefront. An envelope of the secondary wavefronts is the new wavefront (the arc in bold).

A plane wavefront is a referent wavefront against which an arbitrary chosen wavefront is measured.

2.2. A notion ‘aberration’

If the optical media isn’t homogeneous the wavefront is distorted. Any deviation from a plane wavefront is called an aberration. The wavefront can be distorted both when reflecting from an uneven surface or by passing through the media the refractive index and thickness of which changes from point to point (see Figure 2.2.1.). Aberrations modulate the phase of the wavefront. Because of absorbtion the amplitude of light intensity can also vary. Aberrations may origin in any optical media of an eye (a cornea, an anterior chamber, a lens, a vitreous humor).

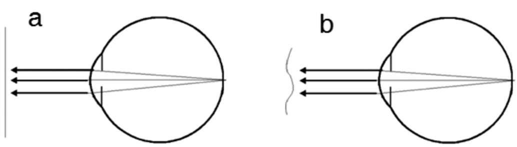

Figure 2.2.1. Plane wavefront (a) and distorted wavefront with aberrations (b). In each optical element of an eye the wavefront is distorted because of different reasons.

Ocular aberrations are classified into two main groups – lower-order and higher-order aberrations. Lower-order aberrations are piston, tip/tilt, defocuss and astigmatism. Piston is simply a delay of the wavefront when passing through a homogeneous media with parallel surfaces. In the case of piston the shape of the wavefront and direction of propagation isn't changed. The shape of the wavefront is preserved also in the case of tip/tilt while the direction of propagation is changed. Any aberration (except piston and tip/tilt) degrades quality of the image formed on the retina and distorts also the outgoing wavefront. Lower-order aberrations can be corrected with galsses and contact lenses while higher-order aberrations can be corrected with adaptive optics, refractive surgery etc.

2.3. The mathematical description of aberrations

Most frequently aberrations are described by using either Zernike's or Seidel's aberration theory [1]. Historically the Zernike's aberration theory has become more popular than the Seidel's theory. According to the Zernike's aberration theory a wavefront can be decomposed into basic types of aberrations. Each basic type of aberration is described by a Zernike polynomial which has two arguments – a radial argument or a radius vector ρ and a polar angle θ (see Figure 2.3.1.).

Each Zernike polynomial has its own Zernike coefficient. The Zernike coefficients are multipliers of corresponding Zernike polynomials and indicate contribution of each type of aberration to the total pattern of aberrations. By using the Zernike polynomials and the Zernike coefficients an arbitrary wavefront W can be written in a form:

$$W(\rho,\theta) = \sum_n^k \sum_{m=-n}^n c_n^m Z_n^m (\rho,\theta) \qquad (2.3.1.)$$

where c_n^m is the Zernike coefficient but Z_n^m is the Zernike polynomial.

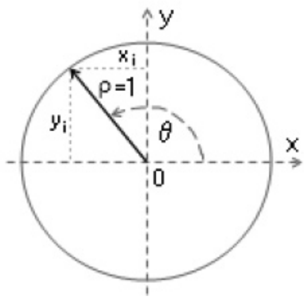

Figure 2.3.1. Arguments of Zernike polynomials – a radius vector ρ and a polar angle θ. The radius vector is a dimensionless parameter and take values between 0 and 1. The polar angle is measured counterclockwise from 0° to 360°.

There are several standards of the Zernike polynomials. Most frequently the OSA (The Optical Society of America) standard is used.

2.4. Formation of an image in an optical system

Let's consider an aperture behind which a converging lens has been placed. An aperture function defined within the aperture is given by an equation [2]:

$$A(y,z) = A_o(y,z) \cdot e^{i\phi(y,z)} \quad (2.4.1.)$$

where $A_o(y, z)$ – the amplitude, $\varphi(y, z)$ – the phase at the point with coordinates (y, z).

The image is formed in the focal plane of the lens. This image is called a point spread function. In the case of coherent radiation the point spread function for the electric field is calculated as a two-dimensional Fourier transform of the aperture function [2]:

$$\mathrm{E}(y, z) = \iint_{-\infty}^{+\infty} A(y,z)\, e^{ik(Y_y+Z_z)/R} dydz \quad (2.4.2.)$$

If a circular aperture is filled with a plane wavefront then the Fraunhofer diffraction pattern (the Airy disc with surrounding periodic light and dark circles) is formed in the focal plane of the lens. The Fraunhofer diffraction pattern is a special case of the point spread function. The radius of the first minimum can be calculated from an equation:

$$r = \frac{1.22 \cdot \lambda}{d}\ (\mathrm{rad}) \quad (2.4.3.)$$

The formation of an image in an optical system can be described as convolution of intensity distribution of the object with the point spread function. Each point is replaced by the point spread function and the final image is the sum of all point spread functions:

$$I_i(Y,Z) = \iint_{-\infty}^{+\infty} I_o(y,z) \cdot S(Y-y, Z-z) dydz = I_o(y,z) \otimes S(y,z) \quad (2.4.4.)$$

where I_i (Y, Z) – distribution of light intensity in the image, $I_o(y, z)$ – distribution of light intensity in the object, S(y,z) – the point spread function, $\otimes$ – a convolution operator.

2.5. Metrics of the optical quality

The metrics most frequently used to describe the optical quality of an optical system are the PV (Peak-to-Valley or the maximal deformation of a wavefront) value, the RMS (the root mean square) value and the Strehl ratio.

The PV is the maximal wavefront deformation. Although the PV can be easy calculated it is not the most suited parameter for describing the optical quality of an optical system. An optical system with a higher PV may perform better than another one the PV of which is lower.

The RMS is the standard error of the wavefront and it is calculated for a pupil with a certain size thus describing the optical quality of an optical system much better.

The RMS can be calculated as the square-root of the sum of the Zernike coefficients squared [3]:

$$\mathrm{RMS} = \sqrt{\sum_{n,m}(c_n^m)^2} \tag{2.5.1.}$$

The Strehl ratio is the ratio of maximal intensity of a point spread function to maximal intensity of the Fraunhofer diffraction pattern. The Strehl ratio can take any value between 0 and 1. If the Strehl ratio equals 1 then the optical system is limited only by diffraction. If the Strehl ratio is 0 then there is zerro energy in the central peak of the point spread function.

A Fourier transform of the point spread function is the optical transfer function (OTF). The optical transfer function has the real part or a modulation transfer function (MTF) and the imaginary part or a phase transfer function (PTF).

2.6. Role of aberrations in vision science

2.6.1. Influence of ocular aberrations on visual perception

The effects of aberrations are usually analyzed together with those of diffraction. If a pupil is small then diffraction plays significant role in blurring an image. Contrary, if the pupil is large then ocular aberrations dominate. Both diffraction and ocular aberrations cause blur of a retinal image and modulate the spectrum of the spatial frequencies. Transmittance of the spatial frequencies are described by the modulation transfer function showing to what extent different spatial frequencies are transmitted by an optical system and what is the ratio of image contrast to object contrast for different spatial frequencies. In real eyes the modulation transfer function falls to zerro at the spatial frequency about 60 cycles/degree.

Dependence of visual perception on ocular aberrations has been widely studied. Ocular aberrations affect visual acuity [4], contrast sensitivity [5, 6], stereo vision [7], accomodation [8] and other visual functions. In the study [4] dependence of visual acuity on higher-order ocular aberrations for different levels of luminance of the stimulus and different polarities of contrast was studied. Significant increase in visual acuity was found in the case of white stimuli shown on a black background irrespective of the luminance level. In other study [9] attention has been paid to dependence of visual acuity on different types of aberrations. Correction of both the second and the third order aberrations caused significant increase in visual acuity whereas correction of the fourth order aberrations didn't result in increase of visual acuity. In the study [5] six-fold reduction in the contrast threshold was reported after correction of higher-order ocular aberrations. An intraocular difference between amount of ocular aberrations influences stereo vision [7]. The stero threshold increased with intraocular difference of amount of ocular aberrations.

Visual perception depends not only on the optical but also on neural factors. The visual cortex that receives information from a retina adapts to the retinal blur caused by ocular aberrations throughout the life. Adaptation of the visual system to the retinal blur has been investigated by several authors [10, 11]. The authors of the study [11] looked for the optimal amount of higher-order aberrations so that quality of the perceived image is the highest. The optical quality of the image was controlled by the adaptive optics. The subjects had to adjust quality of the image until it was the highest. In the whole subjects' group the highest quality of the image corresponded to the residual amount of higher-order aberrations about 12 % of the total amount. The authors of the study [11] explained the results by adaptation of the visual system to the retinal blur caused by higher-order aberrations. The authors also concluded that the optimal amount of higher-order aberrations must be taken into account when undergoing refractive surgery.

2.6.2. Significance of ocular aberrations in ophthalmology

In ophthalmology special attention must be paid to higher-order aberrations the amount of which can be significant compared to that of lower-order aberrations. If only defocus and astigmatism is corrected then individual photoreceptors can't be resolved in retinal images [5, 12]. Correction of ocular higher-order aberrations in ophthalmology is significant to diagnose retinal pathologies, hemorrages, atrophy of photoreceptors etc.

If higher-order ocular aberrations are corrected it is not only possible to image retinal photoreceptors but also epithelium cells of the pigment layer, capillaries, thrombocytes in retinal blood vessels [13] etc. If adaptive optics is combined with doplerography it is possible to measure velocity of leukocytes [14].

Aberrations can cause problems when determining the refractive error using retinoscopy method. Retinoscopy is especially difficult to use in the case of irregular astigmatism and keratoconus. In these cases it is problematically to find the so called neutralization point. If there is irregular astigmatism in an eye the so called scissor reflex may be observable [15, 16]. The cause of the scissor reflex is a particular path of rays because of higher-order ocular aberrations. One part of the pupil is myopic while the other part is hypermetropic. One limb of the scissors is very dark while the other is very bright. In eyes with keratoconus there is large amount of coma resulting in wrapping of the retinal reflex.

2.7. Principle of adaptive optics

The principle behind adaptive optics, i.e., modulation of the phase of the wavefront was first suggested by an American astronomer Horace Welcome Babcock in 1959. As the wavefront travels through the layers of atmosphere it is deformed because of local changes in temperature resulting in slightly changing refraction index. The principle of adaptive optics is shown in Figure 2.7.1. The wavefront is sensed by a wavefront sensor that sends the data further to a computer. The computer in its turn calculates correction algorithms from the sensor data so that the mirror takes the shape needed to make the wavefront plane after reflection. If a plane wavefront is incident upon a focusing system then an image called a diffraction pattern is formed in the focal plane. The principle of adaptive optics is somehow similar to the inverted version of bendy mirrors. A deformed mirror can improve a low-quality image in a way similar to that in which a deformed mirror distorts a high-quality image.

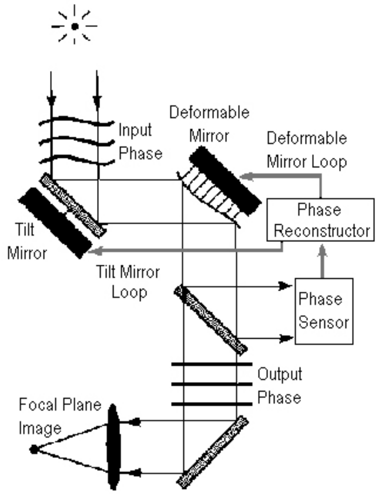

Figure 2.7.1. The principle behind adaptive optics. A plane wavefront is deformed in inhomogeneous optical media. After being reflected by a tilt mirror and a deformable mirror the wavefront enters into a wavefront sensor. The wavefront sensor sends the data to a computer which in its turn controls the shape of the deformable mirror. After being reflected from the deformable mirror the wavefront becomes plane and forms a sharp image in the focal plane [17].

Several years after astronomers started to use adaptive optics vision scientists also found its application for correcting higher-order ocular aberrations. Both in astronomy and in vision science adaptive optics consists of three main blocks:

1. a wavefront sensor;
2. a wavefront modulator and a control block;
3. a software for reconstructing the wavefront and calculating correction algorithms.

Most often a wavefront is analyzed by using a Shack-Hartmann wavefront sensor. The sensing element of the Shack-Hartmann wavefront sensor is a CCD pixel matrix. Apart from the focal system of a digital camera in the Shack-Hartmann sensor a lenslet matrix is used instead of a single lens system. Each lenslet forms a point in the plane of the CCD matrix (see Figure 2.7.2.). If a plane wavefront is incident on the lenslet matrix then the points on the CCD sensor form absolutely symmetric grid in which any two adjacent points are separated by a distance equal to that between the centers of two neighbouring lenslets. If a distorted wavefront is incident on the lenslet matrix then these points deviate away from their initial locations. By measuring these deviations the local slope above the corresponding lenslet is calculated. If the local slope above each lenslet is known the shape of the whole wavefront can be calculated. The wavefront is decomposed into basic types of aberrations. After the wavefront has been reconstructed it is decomposed into Zernike polynomials using the method of least squares.

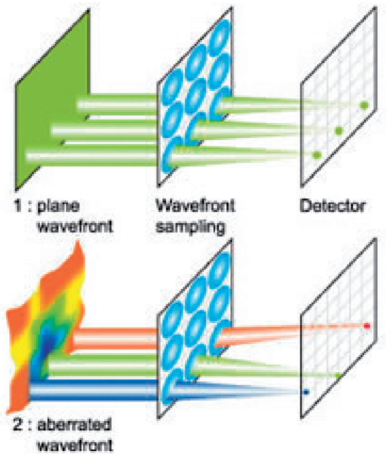

Figure 2.7.2. The principle behind the Shack-Hartmann wavefront sensor. (a) If the wavefront is plane then the distance between two adjacent points equals that between the centres of two adjacent lenslets. (b) If the wavefront is distorted then the distance between two adjacent points is different and depends on curvature of the wavefront [18].

The wavefront corrector adjusts the shape of the wavefront so that it becomes a plane. Different kinds of wavefront correctors exist. Two most popular kinds of wavefront correctors are deformable mirrors and spatial light modulators. Deformable mirrors consist of many separate segments each of which can be pushed or pulled so changing the shape of the wavefront. The principle behind the working of spatial light modulators is changing the refractive index in a liquid crystal matrix.

3. EXPERIMENTAL PART

3.1. Studies of Vernier acuity

3.1.1. Introduction

The visual system is able to detect very small breaks in straight lines. This ability is called Vernier acuity [19, 20]. The Vernier threshold is much lower than the angular distance between two adjacent photoreceptors, i.e., 30′′. The high Vernier acuity can't be explained by the classical theories of visual acuity – Rayleigh criterion and photoreceptor theory. The basis of Vernier acuity is mathematical operations which are performed in the highest centers of the visual system [21]. Vernier acuity is little dependent on defocus [22, 23] and light scattering. In addition, it is known that eye movements improve Vernier acuity in the peripheral field of view [24]. The reason why Vernier acuity is relatively insensitive to the retinal blur is the large number of photoreceptors involved into deriving the location of a line.

There is a hypothesis that if the image on the retina becomes very sharp then the visual system has difficulties when deriving the location of the line resulting in reduction of Vernier acuity [25]. In the doctoral work, this hypothesis was tested using the adaptive optics method. The goal of the study was to investigate whether Vernier acuity depends on the correction level of ocular higher-order aberrations.

3.1.2. The experimental part

3.1.2.1. The optical setup

Dependence of Vernier acuity on the amount of higher-order ocular aberrations was studied by using the optical setup schematically shown in Figure 3.2.2.2.1. For measuring the total aberrations of the optical setup and an eye an infrared laser emitting at λ=850 nm was used as a light source. After being reflected from a retina the beam was expanded to the area of the pupil and was directed out of the eye. For measuring aberrations of the optical system a plane mirror was placed where the eye was previously located. In the next stage of the optical setup defocus was corrected using the Badal system. The Badal system also expanded the beam to the area of the deformable mirror. Next, the beam was reflected by the deformable mirror and was directed into the Shack-Hartmann wavefront sensor. For measuring aberrations of the optical setup a collimated light beam was used. The collimated beam was created by focusing a laser beam (λ = 670 nm) emitted by a solid state laser on the end of a single-mode polarization-maintaining fiber. The beam was focused by the lens L1. The other end of the fiber was placed in the focal plane of the lens L2.

The stimulus was shown on a minidisplay (*Liteye*). The minidisplay was placed in the focal plane of the lens L5. The beam originating from the stimulus was reflected by the deformable mirror and after passing through the Badal system entered into the subject's eye. One pixel of the minidisplay subtended an angle 20″ strongly exceeding the typical tVernier threshold that is about 5″ – 10″. For the minidisplay to be usable in the experiment two flankers were placed on both sides of the stimulus. The flankers are known to elevate the Vernier threshold considerably [26].

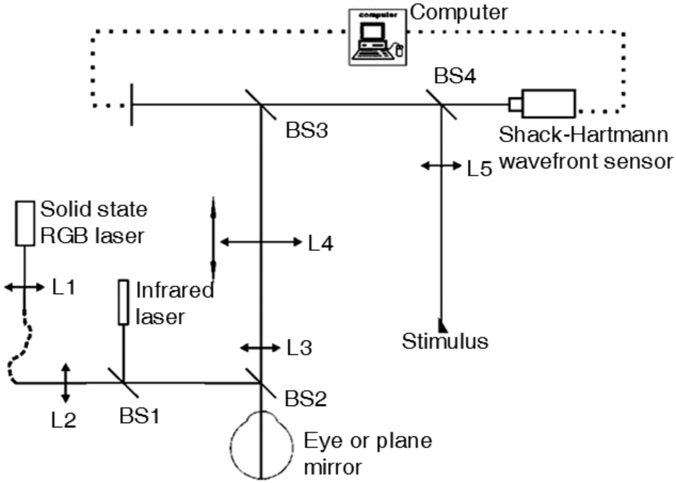

Figure 3.2.2.1.1. The optical setup for measuring Vernier acuity. The optical setup has been described in more details in the text. L – lenses; BS – beam-splitters.

3.1.2.2. Correcting higher-order aberrations

The subjects placed the lenses of the Badal system at such a distance one from another that defocus was minimal and the stimulus was sharp. Next, the sum of ocular aberrations and aberrattions of the optical setup was measured. In the next stage the total aberrations were corrected and the residual aberrations were measured. The voltages applied to the electrodes of the deformable mirror were registered.

In the next stage aberrations of the optical setup were measured. The aberrations were measured when a collimated laser beam was reflected by a plane mirror. The Badal system was not moved. Next, the aberrations of the optical setup were corrected and the residual aberrations were measured. Again, the voltages applied to the electrodes of the deformable mirror were registered.

Using the registered voltages ocular aberrations were corrected at different level.

3.1.2.3. Psychophysical method

The method of constant stimuli was used to measure Vernier acuity. The stimulus was composed of two vertical edges of rectangles. The edges were placed one above another. The lower edge was static while the upper edge could move to the right and to the left. The stimulus was viewed monocularly with the right eye. The subjects had to decide whether the upper edge is to the right or to the left from the static edge. If the subject reported the upper edge to be to the right from the lower edge the key 'L' was pressed and a value '1' was saved, otherwise the key 'K' was pressed and a value '0' was saved.The upper edge had 21 possible position relative to the lower edge. In each position the upper edge was shown 10 times. The position of the upper edge was chosen randomly. For each correction level of higher-order aberrations the experiment was repeated 10 times and from all the measurements the average value and the standard error was calculated. There were altogether 11 correction levels of higher-order aberrations ranging from 0 % to 100 %.

3.1.2.4. Data analysis

The data was analyzed by calculating each subject's psychometric function. The number of times (out of 10) when the subject reported the moveable edge to be to the rigth from the static edge is plotted on the y-axis. The width of the break is plotted on the x-axis. The data was fitted with a Boltzmann sigmoid that was considered to be the subject's psychometric function. The Boltzmann sigmoid is given by an equation:

$$f(x) = A_2 + \frac{A_1 - A_2}{1 + e^{\frac{x - x_0}{\sigma}}} \qquad (3.1.2.4.1.)$$

where A_1 un A_2 – the maximal and the minimal value, respectively, x_o – the x value at which the Boltzmann sigmoid reaches half of its maximal value , σ – the half-width of the sigmoid. In this study $A_1 = 10$ and $A_2 = 0$.

Vernier threshold is the parameter sigma σ of the Boltzmann sigmoid. For every subject the average value of the Vernier threshold was plotted against the level of correction of higher-order ocular aberrations.

3.1.3. Results

3.1.3.1. Effectiveness of correction of higher-order ocular aberrations

In Figure 3.1.3.1.1. it can be seen that for all subjects the point spread function of ocular 3rd and 4th order aberrations became narrower after correction of the aberrations with adaptive optics.

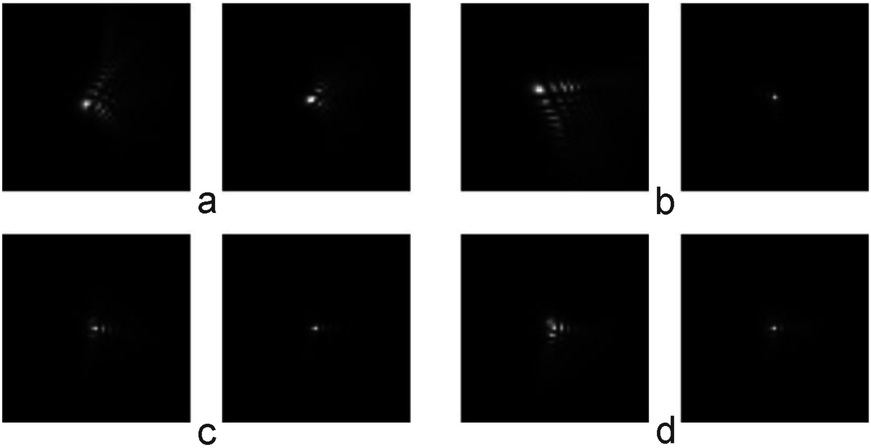

Figure 3.1.3.1.1. The point spread functions of the third and the fourth order ocular aberrations ((a) – VK; (b) – AB; (c) – LE; (d) – IL) before correction and after correction with adaptive optics. The point spread functions have been simulated in Matlab.

3.1.3.2. Dependence of Vernier acuity on the correction level of higher-order aberrations

In Figure 3.1.3.2.1. dependence of the Vernier threshold on the correction level of higher-order aberrations is shown for all subjects. Each data point is the average value of ten measurements while the error bars are the standard error bars.

For three subjects (VK, IL, LE) the Vernier threshold was lower (Vernier acuity higher) in the regions of low and high correction levels compared to the region of medium correction levels. For each of these subjects the RMS of higher-order aberrations corresponding to the highest Vernier threshold was individual: VK: RMS = 0.048 μm; LE: RMS = 0.065 μm; IL: RMS = 0.039 μm.

3.1.4. Analysis

The narrowing of the point spread functions indicate that after correction of higher-order aberrations the number of stimulated photoreceptors is reduced significantly. The results obtained confirm that Vernier acuity depends on the correction level of higher-order aberrations. For three subjects (out of four) Vernier acuity was higher in the regions of low and high correction level of higher-order aberrations compared to the region of medium correction levels. Relatively high Vernier acuity in the region of low correction level can be explained with a large number of photoreceptors contributing to locating the line. It must also be taken into account that if correction level of higher-order aberrations is low then an eye has optical defects which the visual system has adapted to. In this case the

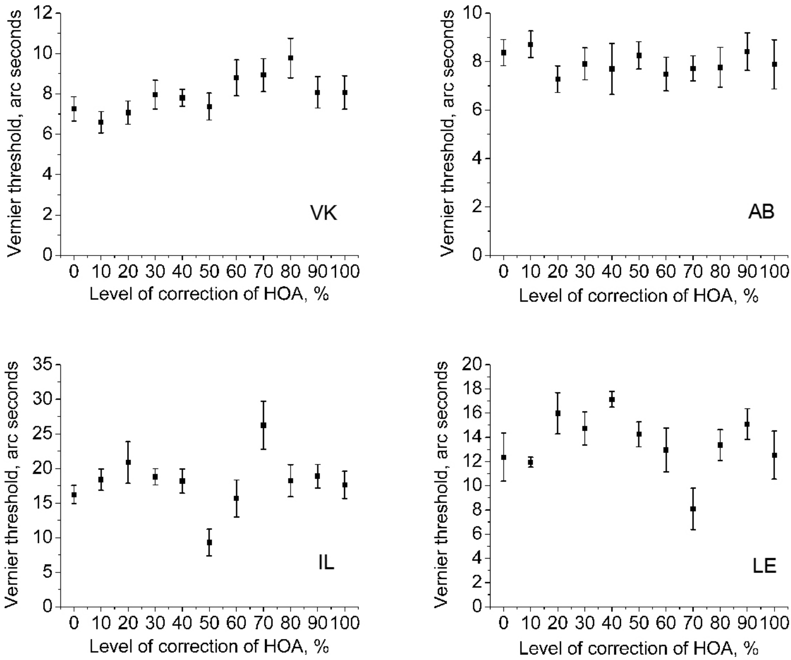

Figure 3.1.3.2.1. Dependence of Vernier acuity on the correction level of higher-order aberrations. On x-axis the correction level of higher-order aberrations in percent is given, on y-axis the Vernier threshold in arc seconds is given.

straight lines are perceived as straight resulting in high Vernier acuity. Relatively high Vernier acuity in the region of high correction level can be explained by high contrast and sharpness of the image formed on the retina.

The relationship between the Vernier threshold and the correction level of higher-order aberrations is somewhat similar to that between the size of a real eye's pupil and its spatial resolution. If the pupil diameter is small, the eye's resolution decreases because of diffraction effects, whereas at a large pupil the resolution decreases owing to aberrations. The optimal size of the pupil is about 3 mm because the total impairment of the image quality because of diffractions and aberrations is the smallest. In a similar way Vernier acuity depends on optical and neural factors.

The deformation amplitude of the deformable mirror was too small to overcorrect higher-order ocular aberrations and investigate the effect of overcorrection on Vernier acuity. The results indicate that below a certain level of overcorrection Vernier acuity may improve and subsequently lower again.

3.2. Influence of ocular aberrations on binocular visual perception

3.2.1. Introduction

Most of the studies regarding influence of the optical quality of an eye on visual perception is carried out monocularly. Ocular aberrations influence not only monocular but also binocular vision. Results obtained in the study [7] confirm that ocular aberrations elevate the stero threshold significantly. It is known that aniseikonia (difference between the images formed onto both retina) can have an effect on binocular vision – if the difference is larger than 10 % then the visual system is unable to fuse them together [27]. Aniseikonia is the consequence of correction of anisometropia (large interocular difference of the refractive error). The images formed in both eyes are incompatible also if one of the images are significantly blurred compared to the other image. In this case the blurred image is ignored. This mechanism is called suppresion.

Influence of ocular aberrations on binocular vision is especially important to those who wear power progressive lenses. Power progressive lenses ensure clear vision at any distance. These lenses are suited for people aged about 40 or more. When looking sideways both eyes look through zones of the lenses which have different types and amount of aberrations. The surface of the power progressive lenses is very complex, and high quality of vision is guaranteed only in the coridor. In the peripheral field of view the image is distorted because of aberrations which arise from rapid variations in curvature of the surface. When starting to wear power progressive lenses objects in the field of view seem to be blurred and curved. An adaptation period is required so that objects are perceived sharp and straight lines are perceived as straight.

In the doctoral work the intraocular RMS difference threshold was measured. This threshold must be exceeded so that the images formed onto retina in both eyes can't be fused together. This study is essential when designing the power progressive lenses because the maximal permissible difference between both images must not be exceeded so that the brain can fuse the images together.

3.2.2. The experimental part

3.2.2.1. The optical setup

The optical setup used in the study is shown schematically in Figure 3.2.2.1.1. The optical setup consisted of two separate paths – one for the left eye and another for the right eye. The stimuli S1 and S2 were placed in the focal planes of aspheric lenses L1 and L2. The stimuli were shown dichoptically, i.e., each eye viewed only its own stimulus. The stimuli were illuminated from back by a superluminiscent red light emitting diode. Black bars on a red background were chosen to minimize the effect of chromatic aberration. After passing through the lens L1 in the optical path of the left eye the rays were reflected by a deformable mirror while in the optical path of the right eye the rays were reflected by a plane mirror. The Badal systems (lenses L3, L4, L5, and L6) compressed the area of the deformable mirror and the plane mirror to that of the pupil and corrected defocus. A screen with apertures ensured that each eye saw only its own stimulus.

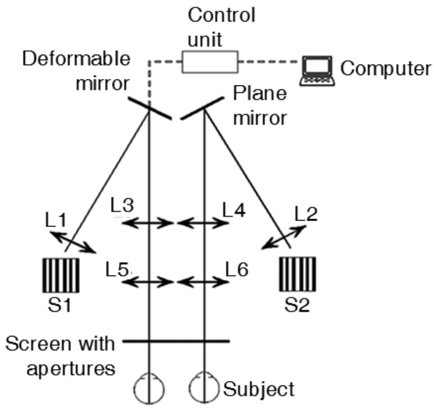

Figure 3.2.2.1.1. The optical setup for studying binocular visual perception. The optical setup has been described in details in the text. L – lenses, S – stimulus.

3.2.2.2. The psychophysical method

The method of constant stimuli was applied to study influence of aberrations on binocular visual. The images were distorted by following types of aberrations: oblique astigmatism c_2^{-2}; vertical coma c_3^{-1}; horizontal trefoil c_3^{3} and spherical aberration c_4^{0}. The experiment is illustrated in Figure 3.2.2.2.1. At the time moment t_1 a square grating was presented to each eye. At this time moment the deformable mirror was plane. At the time moment t_2 the image of the left eye was distorted by a certain type of aberration the amount of which was chosen randomly. The image quality of the right eye was kept constant. At the time moment t_1 both images were similar and the brain was able to fuse them together. When distortions of the right eye's image at the time moment t_2 exceeded a certain threshold a difference between the binocularly perceived images at the time moments t_1 and t_2 could be noticed.

For all subjects and types of aberrations the intraocular RMS difference threshold was found. This threshold had to be exceeded so that difference between the binocular images at the time moments t_1 and t_2 could be noticed. For each type of aberration there were 11 levels of the RMS and for each RMS value the images had to be compared 10 times. The subject's task was to give an answer to a question whether the binocular image at the time moment t_2 was different from that at the time moment t_1. The experimental room was dark so that other stimuli in the field of view didn't distract subject's attention.

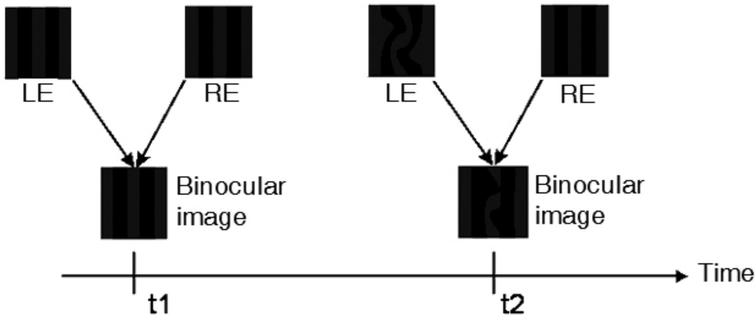

Figure 3.2.2.2.1. The stimuli and the sequence of demonstration for studies of binocular visual perception. At the time moment t_1 the images formed on both retina (LE – the left image, RE – the right image) were equal. The brain fused both images together and these were perceived as a single binocular image. At the time moment t_2 the image of the right eye was the same whereas that of the left eye was distorted by a certain type of aberration. The task was to indicate whether there is any difference between the binocular images seen at the time moments t_1 and t_2.

3.2.2.3. Data analysis

The number of times (out of 10) when the subject reported a difference between both images was plotted vs percent of the maximal RMS value of an aberration. The data was fitted with a Boltzmann sigmoid. The Boltzmann sigmoid was assumed to be the subject's psychometric function. The Boltzmann sigmoid is given by an equation:

$$f(x) = A_2 + \frac{A_1 - A_2}{1 + e^{\frac{x - x_0}{\sigma}}} \qquad (3.2.2.3.1.)$$

where A_1 and A_2 is the maximal and minimal value of the Boltzmann sigmoid, x_o is the x value at which the Boltzmann sigmoid reaches 50 % of its maximal value, σ is the half-width of the Boltzmann sigmoid. In this study $A_1 = 10$ and $A_2 = 0$.

The x value x_o corresponding to 50 % of the maximal value of the Boltzmann sigmoid was assumed to be the intraocular RMS difference threshold. The threshold was measured for different aberrations (oblique astigmatism c_2^{-2}; vertical coma c_3^{-1}; horizontal trefoil c_3^3 and spherical aberration c_4^0).

3.2.3. Results

3.2.3.1. Generation of aberrations

The wavefronts of the generated aberrations and the corresponding interferograms are shown in Figure 3.2.3.1.1. The Zernike coefficients of the generated aberrations are as follow: spherical aberration c_4^0 RMS = 0.7 μm, vertical coma c_3^{-1} RMS = 0.43 μm, oblique astigmatism c_2^{-2} RMS = 0.56 μm and horizontal trefoil c_3^3 RMS = 0.23 μm. This is the largest amount of aberrations that can be generated with the deformable mirror.

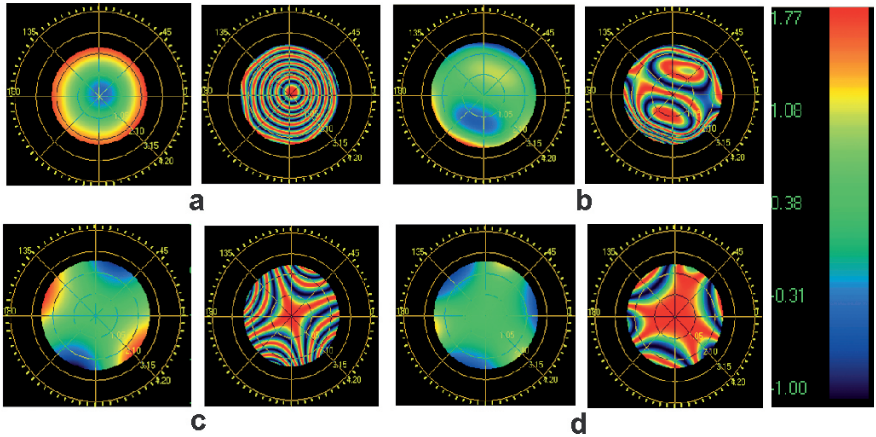

Figure 3.2.3.1.1. The wavefronts generated with the deformable mirror and corresponding interferograms. (a) spherical aberration; (b) vertical coma; (c) oblique astigmatism; (d) horizontal trefoil. Deviation of the wavefront in micrometers can be determined using the colour scale at the right side.

The deviation at each point of the wavefront can be determined by using the coloured scale at the right side of Figure 3.2.3.1.1. The aberrations were measured for the pupil size 5 mm using the Shack-Hartmann wavefront sensor.

3.2.3.2. The intraocular RMS difference threshold

In Table 3.2.3.2.1. the intraocular RMS difference thresholds for all aberrations are summarized. This threshold must be exceeded so that difference between both images can be noticed. The threshold values are calculated by averaging 15 subjects' data. The standard error is given as well.

Table 3.2.3.2.1. The intraocular RMS difference threshold for all types of aberrations.

Type of aberration	The intraocular RMS difference threshold, μm
Astigmatism	0.154±0.010
Spherical aberration	0.204±0.014
Coma	0.126±0.008
Trefoil	0.105±0.007

3.2.4. Analysis

In Table 3.2.3.2.1. it can be seen that in the case of different aberrations the intraocular RMS difference threshold is also different. The highest threshold is observed in the case of spherical aberration whereas it is the lowest in the case of trefoil. The differences in the thresholds may be explained on the basis of adaptation of the binocular visual system to the blur caused by these aberrations.

As mentioned before not only types of aberrations and their amount play a role in visual perception. Adaptation processes must also be taken into account [10, 11]. In the studies [10, 11] adaptation of the visual system to the optical quality of an eye has been studied monocularly. In the doctoral work the results obtained point to the role of adaptation processes in binocular vision. The role of adaptation processes in binocular vision is confirmed by the results obtained in the study [28]. The authors of the study [28] observed that when a subject has adapted binocularly to a blurred or a sharp image for a certain time period sharpness of the perceived image is changes.

The extent to which the binocular visual system has been adapted to the blur caused by specific types of aberrations depends on the symmetry of the wavefront and amount of aberrations. As the cornea is spherical it has some spherical aberration. As the wavefront of spherical aberration is symmetric a human adapts to this type of aberration significantly throughout the life. Because of adaptation a large amount of spherical aberration is needed so that the subject can perceive differences between the binocularly perceived images. The optimal amount of spherical aberration exists [29]. This is the amount of spherical aberration at which visual performance reaches its highest level. Other types of aberrations (for example, coma) have asymmetrical point spread functions and thus a smaller intraocular RMS difference is needed so that the subject can perceive differences between the two images. When interpreting the results it must be taken into account that ocular aberrations were not corrected and were summed with those generated with the deformable mirror. However, these effects were small because the pupil size was 5 mm and the amount of higher-order ocular aberrations is small for such size of the pupil.

The results obtained can be used when designing power progressive lenses. During design process care must be taken so that when looking through different zones of the power progressive lenses the intraocular difference between the amount of aberrations doesn't exceed that measured in the doctoral work. The results may also be useful for developing new tests to assess binocular visual functions.

3.3. Studies of saturation adaptation

3.3.1. Introduction

Sensory adaptation is a common feature of all sensory systems including the visual system. Sensory adaptation adjusts the sensitivity threshold of photoreceptors [30, 31, 32, 33]. The resultant relationship between a response of a sensory system to an input signal may be complex and depends on the response of each subsystem.

What regards to vision, sensory adaptation may be divided into several classes – luminance adaptation, chromatic adaptation, contrast adaptation etc. Chromatic adaptation in a special kind of luminance adaptation and it influences color vision [34]. The basis of chromatic adaptation is regulation of sensitivity of each class of photoreceptors independently according to intensity of surrounding light. Regulation of sensitivity is accomplished by controlling the gain of the response of photoreceptors. The gain control is modelled by the Michaelis-Menten equation and the Von Kries model and is non-linear [35, 36, 37]. Two well-known colour vision effects – the Bezold-Brücke and the Abney effect result from non-linear characteristics of the human visual system.

There are almost no studies investigating the effect of chromatic adaptation on perceived colour purity. Color purity is a term related to how saturated the color is perceived by a subject. Essentially, the terms 'purity' and 'saturation' are equal the only difference being that the term 'purity' is related to visual perception whereas the term 'saturation' is an objective term. In the doctoral work dependence of purity of chromatic stimuli on chromatic adaptation was studied. In order to avoid possible confusion of purity and hue the adapting and the test stimuli were chosen so that these lied on the same axis joining the white-point and the location of the red phosphor. As the adapting and test stimuli had one and the same hue but different saturation such a type of chromatic adaptation was called saturation adaptation. As a measure of saturation the length of vector joining the white point and location of the stimulus in the CIE diagram was chosen. It was expressed as percentage of the length of the vector joining the white point and the red phosphor.

In the doctoral work perceived purity of two stimuli (a referent and a matching stimulus) under different states of chromatic adaptation was compared. Under all states of chromatic adaptation the point of subjective equality (PSE) defined as condition when the subject perceives both stimuli equally pure was determined. In the doctoral work it was hypothesized that saturation adaptation is non-linear in the same way as the Bezold-Brücke and the Abney effect are. The time course of saturation adaptation was measured. It was also analyzed wherein the visual system the processes related to saturation adaptation may be located.

3.3.2. The experimental part

3.3.2.1. The psyhcophysical method

3.3.2.1.1. Procedure – the method of adjustment

During the whole experiment the subject fixated a small white dot. The experiment started with a blank screen lasting for 10 s which was followed by a demonstration of the referent and the matching stimulus. Saturation of the referent stimulus S_R was kept constant all the time. As the time progressed saturation of the matching stimulus S_M either decreased from 1 to 0.5 or increased from 0.5 to 1 linearly at rate 0.05/s (see Figure 3.3.2.1.1.1.). At the time moment $t = t_o$ the subject had reached the PSE. At the PSE a difference

$$D = S_R - S_M \qquad (3.3.2.1.1.1.)$$

was defined. The experiment with the method of adjustment was performed for S_R values ranging from 0.7 to 0.95 in steps of 0.05. For each value of S_R the adjustment procedure was repeated for 10 times.

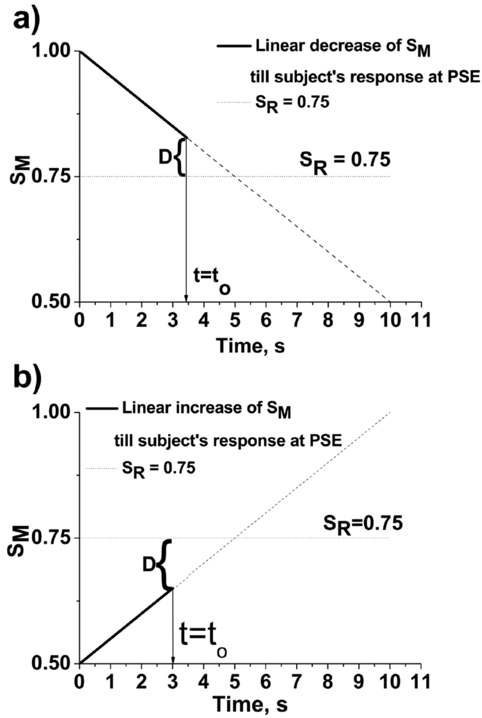

Figure 3.3.2.1.1.1. Procedure in the experiment with the method of adjustment. At time moment t = 0 saturation of the matching stimulus S_M started either to decrease – upper diagram (a); or increase – lower diagram (b). Saturation of the referent stimulus S_R was always kept constant.

3.3.2.1.2. A procedure – the method of constant stimuli

To determine characteristics of the time course of saturation adaptation the method of constant stimuli was used. As in the previous experiment the subject fixated a small white dot during the whole experiment. The experiment consisted of 3 separate phases as shown in Figure 3.3.2.1.2.1. – 1) blank screen; 2) adapting phase t_a; 3) test phase t_t. The blank screen lasted for a period t_b = 10 s. During the adapting phase the subject saw the referent stimulus with $S_R = 0.75$ and the adapting stimulus with $S_M = 0.5$. Duration of the adapting phase varied from 0.25 s to 1.25 s in steps of 0.25 s. The adapting phase was followed by the test phase. The start moment of the test phase was marked by a loud beep. During the test phase the subject saw the referent stimulus with $S_R = 0.75$ and the matching stimulus. Saturation of the matching stimulus S_M varied stepwise from 0.5 to 1 in steps of 1/36. As the test phase started the subject had to give an answer to a question whether the matching stimulus looked more pure than the referent stimulus, or not. By using the collected data psychometric functions were measured and the difference $D = S_R - S_M$ was found at the PSE.

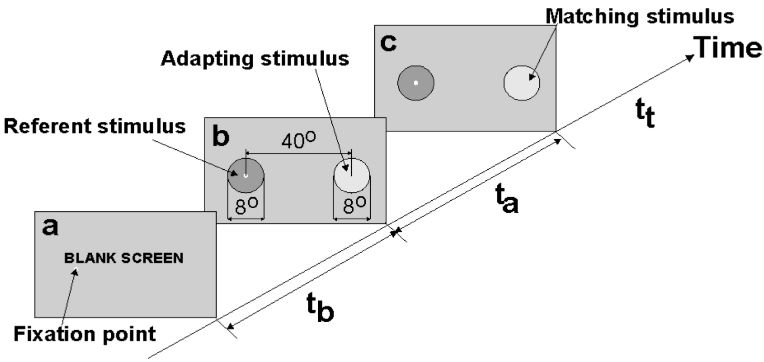

Figure 3.3.2.1.2.1. The sequence of phases in the experiment with the method of constant stimuli. a) – blank screen lasting for t_b = 10 s; b) – adapting phase t_a; c) – test phase t_t .

3.3.2.2. Stimuli

In both psychophysical methods of our studies a referent and a matching stimulus were used. Both stimuli were uniformly coloured with the angular size of each stimulus 8° as viewed from distance 40 cm. The centres of both stimuli were 40° apart from each other. Stimuli were viewed against a black background and the subject had to fixate a small white dot at the centre of the referent stimulus. The subject was adapted under different conditions, *i.e.*, the referent stimulus was more saturated than the matching stimulus, or vice versa. In one of the experiments the referent stimulus had constant saturation while saturation of the matching stimulus changed linearly. In the second experiment both stimuli had constant saturation during the adapting phase but the duration of the adapting phase could be varied. During the experiments chromatic coordinates of both stimuli were modulated along the axis joining the white point and the red phosphor. Luminance of both the referent and the matching stimulus was kept constant **Y** = 40 cd/m^2. The room was darkened and illumination was 20 lx so that peripheral stimuli didn't distract subject's attention from the stimuli. The walls of the room were neutral grey.

3.3.3. Results

3.3.3.1. The method of adjustment

Dependence of the difference D on saturation of the referent stimulus S_R for both directions of adjustment (S_M increases or decreases) is shown in Figure 3.3.3.1.1. The black circles show the results when saturation of the matching stimulus increased from 0.5 to 1 while the black squares show results for the opposite direction of adjustment. On x-axis saturation of the referent stimulus S_R is given. For all S_R values there was a gap between S_M values obtained when performing adjustment procedure from both sides of S_R. The error bars shown in Figure 3.3.3.1.1. are the standard error bars.

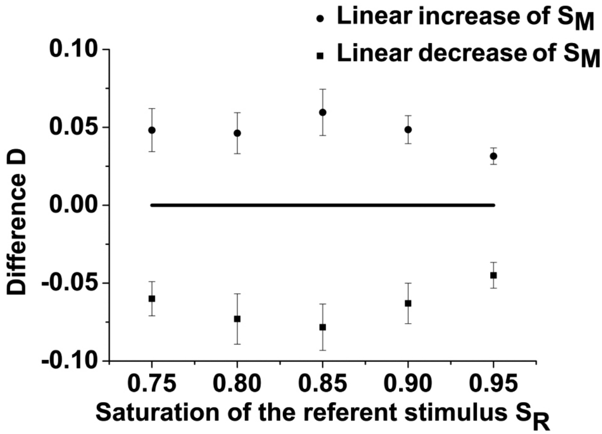

Figure 3.3.3.1.1. The relationship between the difference D and saturation of the referent stimulus S_R at the point of subjective equality. Circles are data for case when the saturation of the matching stimulus S_M varies from 0.5 to 1. Squares are data for case when saturation of the matching stimulus S_M varies from 1 to 0.5.

3.3.3.2. The method of constant stimuli

The data obtained was fitted with a Boltzmann sigmoid. The sigmoid was assumed to be the subject's psychometric function. The sigmoids are shown as the solid lines in Figure 3.3.3.2.1. On y-axis a fraction F is given showing how many times (out of 10) the subject responded the matching stimulus to look more pure than the referent stimulus. On x-axis the difference between S_M and S_R is given. At the PSE a psychometric function has a value 0.5 and the D value at the PSE can be read from x-axis.

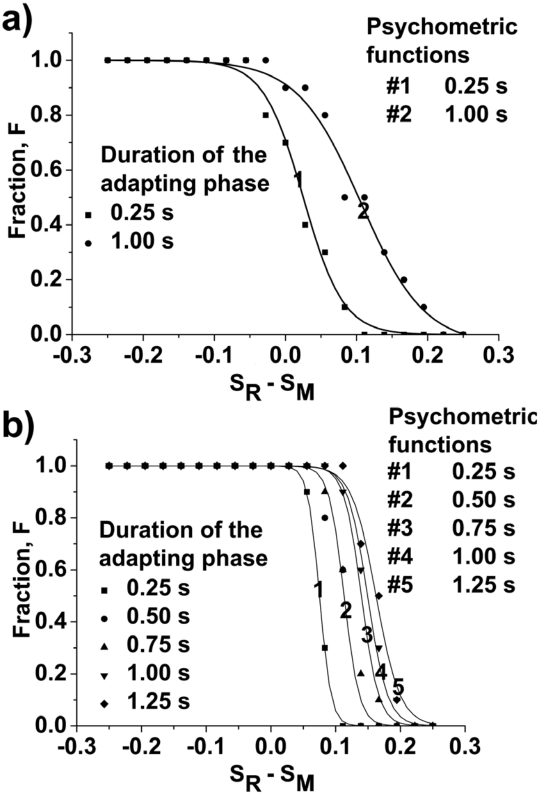

Figure 3.3.3.2.1. The psychometric functions measred in the experiment with the method of constant stimuli. Duration of the adapting phase was variable. In the panel (a) the psychometric functions obtained by averaging all subjects' data are shown. Durations of the adapting phase was 0.25 s and 1 s. In the panel (b) the subject's VK psychometric functions are shown. Duration of the adapting phase varied from 0.25 s to 1.25 s (in steps of 0.25 s).

The shift of psychometric functions caused by increasing duration of the adapting phase is clearly visible. At the upper diagram (Figure 3.3.3.2.1. a) the mean shift averaged across all subjects is shown whereas at the lower diagram of (Figure 3.3.3.2.1. b) the shift of psychometric functions is shown for the subject VK. For all subjects the data was obtained only for durations of the adapting phase 0.25 s and 1 s. The subject VK was measured under conditions when duration of the adapting phase increased from 0.25 s to 1.25 s in steps of 0.25 s. In Figure 3.3.3.2.2. the value of the difference D at the PSE versus duration of adapting phase is shown. Relationship between the difference D and duration of the adapting phase was expected to be non-linear and was fitted with an exponential growth function of type:

$$D = D_1 + D_2 \cdot (1 - e^{-\frac{t}{\tau}}) \quad (3.3.3.2.1.)$$

where $\mathbf{D_1}$ and $\mathbf{D_2}$ are constants, $\boldsymbol{\tau}$ is a half-life of the time course of saturation adaptation. The half-life $\boldsymbol{\tau}$ is a time period after which the value of $D_2\exp(-t/\tau)$ has decreased e times compared to the value at the time moment $\mathbf{t} = 0$. The obtained half-life value of saturation adaptation $\boldsymbol{\tau} = 0.81$ s.

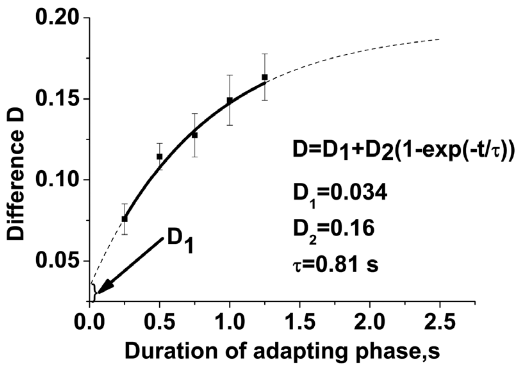

Figure 3.3.3.2.2. Dependence of the difference D = S_R – S_M = 0.75 – S_M on duration of the adapting phase. The solid line is an exponential function that was fitted to the data. The values of the function are shown in an interval from the shortest to the longest adapting phase. The dashed line is a continuation of the exponential function outside the studied duration of the adapting phase.

3.3.4. Analysis

Hysteresis of the difference D in the experiment with the method of adjustment was observed. Obviously hysteresis is due to different conditions of chromatic adaptation when performing the adjustment from both sides of saturation of the referent stimulus. As can be seen from Figure 3 the amount of hysteresis can't be described by any function but is steady observable across a range of S_R values.

In the doctoral work the time course of saturation adaptation was measured by analysing dependence of the difference D on duration of the adapting phase. The dependence could be well fitted with an exponential growth function similar to that suggested by Keller et al. [38] in his article regarding enzyme kinetics. The successful fit with the exponential function may be consequence of enzymatic processes occurring in the photoreceptors. The chain of the phototransduction cascade is too complicated for specific reactions to be identified as possible sources of the exponential relationship. Other visual subsystems could also be involved in the exponential character of the relationship as well. Additional experiments must be done to find the key reactions responsible for this type of relationship. As the calcium is one of the most important chemical elements involved in adaptation processes two most basic enzymatic processes controlling the opening and the closure of the Ca channels (cGMP channels) seem to be related to the exponential character of the relationship. One such process is GTP hydrolysis by guanylcyclase into cGMP. The second process is converting cGMP to GMP by phosphodiesterase [33, 39].

Several authors have measured the time course of chromatic adaptation already previously. Rinner and Gegenfurtner [40] measured the impact of adaptation to chromatic background on colour appearance and colour discrimination. The authors of the study [40] plotted adaptation state (expressed in %) versus time after stimulus onset. They resolved three distinct half-life components in the time course of chromatic adaptation for both colour appearance and colour discrimination. Different half-life values point to various locations of processes involved in the processes of the chromatic adaptation and to that the visual system can't be considered as a single circuit and must be divided into subsystems each of which has different time course. The visual system can be divided into several subsystems each of which has its own half-life values in chromatic adaptation. The authors suggested that the mechanism of the slowest component (half-life value 20 s) may be located in retina, geniculate bodies or early cortical level. The second component had a half-life about 40 ms to 70 ms. Authors identified the photoreceptors as the most likely location where this fast component could be located. The third component with a half-life about 10 ms was supposed to be located in visual cortex. The half-life value τ=0.81 s obtained in our study is obviously longer than the extremely short life-time (10 ms) of the Rinner's (18) study but considerable shorter than the long half-life (50 s). The half-life value obtained in the doctoral work is the closest to the value 40 ms – 70 ms and therefore it can be suggested that the processes responsible for the exponential relationship are located in photoreceptors.

Similarly to Rinner and Gegenfurtner the time course of chromatic adaptation was also determined by Fairchild and Reniff [41]. Fairchild and Reniff adapted the subject to different illuminants: D65, A, D90 and GRN which changed each other in sequence after certain periods of time. Under each state of adaptation the subject adjusted chromaticity of the test stimulus until it looked achromatic. The proportional movement of adjusted chromaticity was plotted against duration of the adapting phase. The data was successfully fitted with a sum of two exponential functions. The authors obtained half-life values about 1 s for the faster component and 40-50 seconds for the slower component. The authors concluded that the mechanism of both components may be located at retinal level. The half-life value obtained in our study τ = 0.81 s is very close to that of the faster component in Fairchild's and Reniff's [41] study suggesting even more that the enzymatic processes may be located in photoreceptors.

3.4. Influence of aberrations on the diameter of retinal blood vessels

3.4.1. Introduction

There are almost no studies investigating how the optical quality of an eye influences appearance of major retinal structures – the optic disc, retinal blood vessels, nerves etc. In the doctoral work attention has been paid to how different aberration patterns influence the apparent diameter (further in the text simply 'diameter') of the retinal blood vessels. The apparent diameter can be different from the actual diameter because of ocular aberrations. In ophthalmology, the A/V ratio is a significant parameter and it is evaluated routinely during each visit to an ophthalmologist. Normally the A/V ratio falls within the range between 2/3 and 4/5. The A/V ratio is assessed when the pupil is dilated. Under this condition there is a considerable amout of ocular aberrations which can significantly influence the A/V ratio. The diameter of retinal blood vessels is related not only to health of the retina but it may also be related to general health of the body.

In the doctoral work a hypothesis was tested that because of aberrations the A/V ratio may be under- or overestimated. In addition, incorrect assessment of the A/V ratio may result in missing pathologies affecting the A/V ratio.

3.4.2. The experimental part

3.4.2.1. Simulation of aberrations in a star chart

In order to assess increase in the line width due to aberrations a star chart method was used.

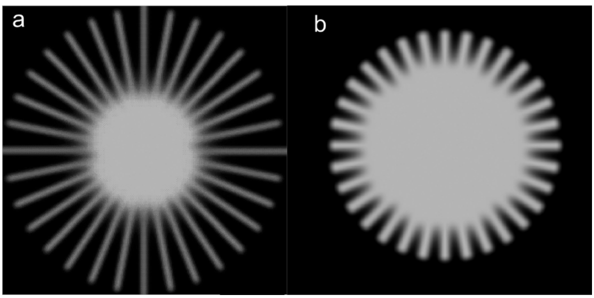

Figure 3.4.2.1.1. The star chart used to evaluate influence of different types of aberrations on increase of the line width. (a) The star chart with wide lines. (b) The star chart with narrow lines.

Lines with a Gaussian profile and the full width at half maximum 13 pixels and 22 pixels were orientated at 16 various directions (see Figure 3.4.2.1.1.). The lines were achromatic (RGB = 128,128,128) and were shown on a black background (RGB = 0,0,0). The direction of the vertical line was assumed to be 0° and the direction of each subsequent line increased clockwise by 11.25°. Following types of aberrations were simulated in the star chart: horizontal astigmatism c_2^2, vertical coma c_3^{-1} and horizontal trefoil c_3^3. The wavefronts and the point spread functions were calculated for the following RMS: 0.1 μm; 0.2 μm un 0.3 μm. The calculations were done for the pupil size 6 mm.

3.4.2.2. Simulation of aberrations in a retinal image

Influence of aberrations on the diameter of retinal blood vessels was evaluated by simulating aberrations in a retinal image. For simulation purposes the retinal image acquired by Prof. Austin Roorda with the adaptive optics scanning laser ophthalmoscopy method was used (see Figure 3.4.2.2.1.) [42]. A written permission to use this image for simulation purposes was received from Prof. Austin Roorda. The retinal area shown in the image is located about 4.5 degrees superior to the fovea. The diameter of the blood vessels seen in the retinal image is about 50 μm.

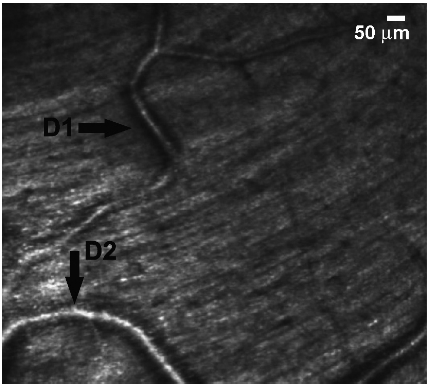

Figure 3.4.2.2.1. The retinal image used for simulation of aberrations. The image was obtained by prof. Austin Roorda using the adaptive optics scanning laser ophthalmoscopy method [87].

Different aberration patterns characteristic to specific groups of people were simulated in the retinal image:

1. Children with high degree of hypermetropia [43];
2. Patients with intraocular lenses [44];
3. Keratoconus patients [45];
4. Subjects with supernormal vision [46];
5. Myopic adults [47];
6. Two groups of normal adults [48].

As the values of all Zernike coefficients were not available for any group then missing information was taken from the study [48]. In the study [48] the values of Zernike coefficients were measured in a large emmetropic population up to the 4th order. The calculations were done for 6 mm pupil. The diameter D1 and D2 were measured at the sites identified by the black arrows and the diameter ratio D1/D2 was calculated.

3.4.2.3. Calculation of the line width and the diameter of the retinal blood vessel

3.4.2.3.1. Full width at half maximum

Both the line width and the diameter of the blood vessels in the retinal image were calculated as the full width at half maximum of the cross-section of the line or the blood vessel. In Figure intensity distribution along the cross-section of the retinal blood vessel is shown. On x axis linear coordinates in μm are given. In the same way the lime width in the star chart was also calculated for every combination of line direction, the type of aberration and the amount of the aberration.

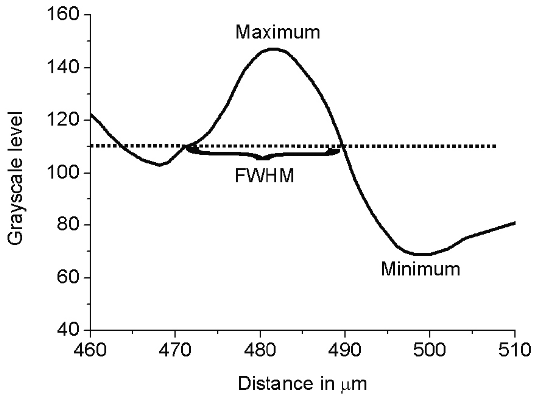

Figure 3.4.2.3.1.1. Grayscale intensity distributed along the cross-section of a retinal blood vessel. The measure of the diameter of the retinal blood vessel was the full width at half maximum.

3.4.2.3.2. An edge detection method

Software that is intended for analyzing retinal images uses edge detection algorithms to find the edges of retinal blood vessels. In order to determine whether edge detection algorithms are sensitive to the aberration effects the diameter of retinal blood vessels was calculated by using the Kirsch edge detection algorithm.

The previously mentioned aberration patterns were simulated in the retinal image again. Apart from the method in which the full width at half maximum was used as the measure of the diameter of a retinal blood vessel in this method the Kirsch edge detection algorithm was used. The basis of the Kirsch edge detection algorithm is calculating the first derivative in certain directions and determining the gradient. The threshold of the Kirsch edge detector was chosen so that the blood vessels were not terminated anywhere. In Figure 3.4.2.3.2.1. two images are shown for comparison purposes. One of the images was used in the method of the full width at half maximum while the other was used in the edge detection method. After converting the image into a binary format the blood vessels were cut manually. By using the intensity profile obtained the diameter of the retinal blood vessels was calculated. The diameter of both blood vessels was calculated and the diameter ratio D1/D2 was calculated.

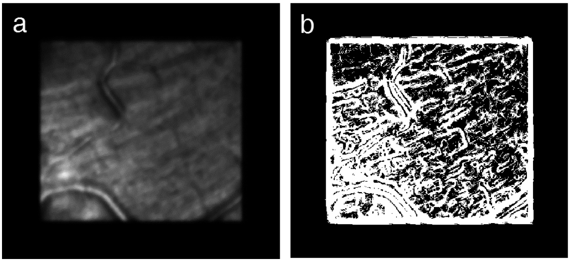

Figure 3.4.2.3.2.1. The retinal images for calculating the diameter of retinal blood vessels. (a) The full width at half maximum. (b) The edge detection method.

3.4.2.4. Correlation between the ratio of the line width and the diameter ratio of the retinal blood vessels

The aberration patterns simulated in the retinal image were simulated also in the star chart. In order to assess the relationship between influence of different aberration patterns on the ratio of the line widths and the ratio of the diameters of the blood vessels the width of the line oriented at 146.25° direction was divided by the width of the line orientated at 90°. The narrow line is an analogue to the narrow blood vessel the diameter of which is D1 whereas the wide line is analogue to the wide blood vessel the diameter of which is D2 (see Figure 3.4.2.4.1.). The ratio of the line width was calculated for every aberration pattern. Correlation between the ratio of the widths of the lines and that of the blood vessels was calculated.

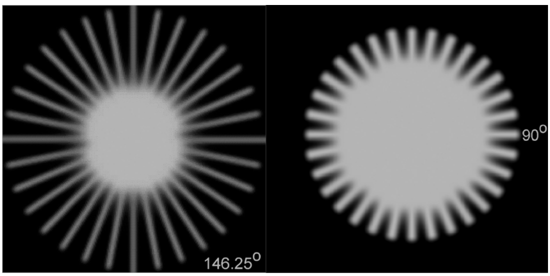

Figre 3.4.2.4.1. Calculating the diameter ratio of the line width for different aberration patterns. The narrow line is analogue to the blood vessel with the diameter D1 whereas the wide line is analogue to the blood vessel with the diameter D2. Orientation of the narrow line is at 146.25° while that of the wide line is 90°.

3.4.3. Results

3.4.3.1. Increase in the line width of the star chart

Increase in the line width of the star chart due to the simulated aberrations is shown in Figure 3.4.3.1.1.

The results are shown for horizontal astigmatism c_2^2, vertical coma c_3^{-1} and horizontal trefoil c_3^3 (the full width at half-maximum is 13 pixels). The results are shown in the polar coordinate system. The radius vector shows how many times the line width increased because of the aberrations. The polar angle increases clockwise and points to orientation of the line.

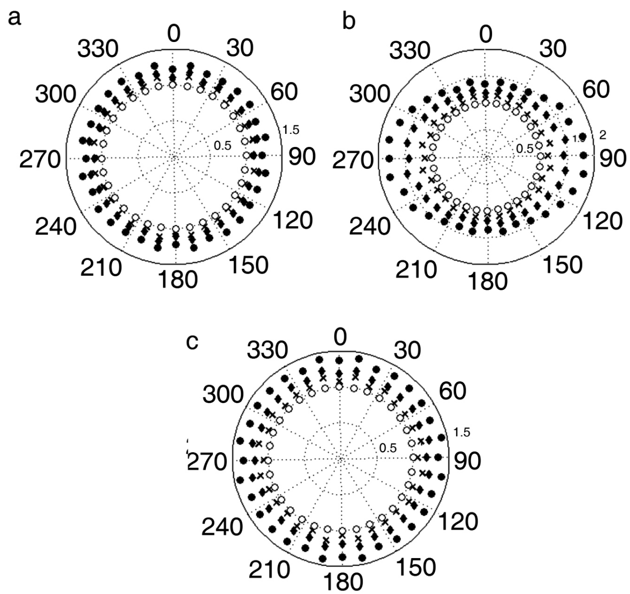

Figure 3.4.3.1.1. Dependence of increase in the line width on orientation of the line. The panel (a) is shown for horizontal astigmatism , the panel (b) is shown for vertical coma , the panel (c) is shown for horizontal trefoil . The plots are shown for the narrow line with the full width at half maximum 13 pixels. The empty circles are show for the case when no aberrations are simulated in the star chart. The crosses are for the RMS = 0.1 µm, the diamonds – 0.2 µm, filed circles – 0.3 µm.

It can be seen that aberrations with different symmetry of the wavefront have also different effect on increase of the line width. Increase in the line width depends not only on symmetry of a wavefront and amount of an aberration but also on the actual width of a line and its orientation. The largest change in the line width is observed in the case of coma because of its asymmetrical wavefront. Contrary to that, the smallest change is observed in the case of astigmatism. Independently on the type and amount of an aberration in the case of the wide line (the full width at half maximum 22 pixels) the increase in the line width changed wihin a much narrower interval.

3.4.3.2. Influence of different aberration patterns on the ratio of the diameter of retinal blood vessels

3.4.3.2.1. Full width at half maximum

In Table 3.4.3.2.1.1. the diameter ratio D1/D2 is shown for all aberration patterns. In the table it can be seen that the diameter ratio varies within a broad range – the amplitude of the change is about 0.5 that is clinically significant amount. In the case of severe pathologies the A/V ratio can be changed by much smaller amount.

Table 3.4.3.2.1.1. The diameter ratio D1/D2 for different aberration patterns. The diameter ratio has been calculated using the full width at half maximum.

Subjects' group	D1/D2
Children with high degree of hypermetropia	0.70
Patients with intraocular lenses	1.02*
Keratoconus patients	0.73*
Subjects with supernormal vision	0.98
Myopic adults	0.88
Normal adults [1st group]	0.67
Normal adults [2nd group]	0.58
Aberration-free state	0.70

*The full width was used instead of the full width at half maximum.

In Figure 3.4.3.2.1.1. influence of two different aberration patterns (subjects with very high visual acuity (A) and the second adult group (B)) on the diameter of the blood vessels is shown. It can be seen that the diameter D1 is larger in the group the members of which have very high visual acuity whereas the diameter D2 is larger in the second adult group.

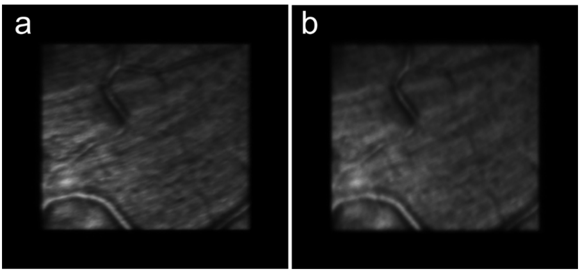

Figure 3.4.3.2.1.1. Influence of aberrations on the diameter of the blood vessels in the group the members of which have supernormal vision (a) and in the second adult group (b). The diameter D1 is larger in the group with supernormal vision whereas the diameter D2 is larger in the second adult group.

3.4.3.2.2. The edge detection method

The ratio of the blood vessels calculated using the full width at half-maximum and the edge detection method is shown in Table 3.4.3.2.2.1.

Table 3.4.3.2.2.1. The diameter ratio D1/D2 for different aberration patterns calculated using the full width at half maximum and the edge detection method.

Subjects' group	D1/D2 (the full width at half maximum)	D1/D2 (the edge detection method)
Children with high degree of hypermetropia	0.70	0.58
Subjects with supernormal vision	0.98	0.78
Myopic adults	0.88	0.88
Normal adults [1st group]	0.67	0.68
Normal adults [2nd group]	0.58	0.43
Aberration-free state	0.70	0.67

For the keratoconus patients and the subjects with intraocular lenses implanted the diameter of the blood vessels couldn't be calculated using the edge detection method because the blur of the retinal image was so large that the blood vessels couldn't be detected.

3.4.3.3. Correlation between the ratio of the line width and the ratio of the diameter of the blood vessels

In Table 3.4.3.3.1. the ratio of the line width and the ratio of the diameter of the blood vessels calculated using the full width at half maximum has been summarized for all aberration patterns.

Table 3.4.3.3.1. The ratio of the line widths and the ratio of the blood vessels calculated by using the full width at half-maximum.

Subjects' group	The ratio of the line widths	D1/D2(the full width at half maximm)
Children with high degree of hypermetropia	0.66	0.70
Patients with intraocular lenses	0.94	1.02*
Keratoconus patients	0.76	0.73*
Subjects with supernormal vision	0.74	0.98
Myopic adults	0.72	0.88
Normal adults [1st group]	0.69	0.67
Normal adults [2nd group]	0.65	0.58
Aberration-free state	0.66	0.70

* The full width was used instead of the full width at half maximum.

3.4.4. Analysis

The experiments with the star chart show that certain types of aberrations influence distribution of light intensity of lines orientated in various directions differently. In addition, the broadening effect depends not only on orientation of the line but also on the initial width of that line. The relative broadening effect is reduced, as the actual line width increases.

Simulation of aberrations in the star chart and the retinal image confirms that ocular aberrations can influence the A/V ratio significantly. Generally, veins are broader than arteries. Based on the results obtained from simulation of aberrations in the star chart it can be concluded that the broadening effect is more marked to arteries compared to veins. It can also be concluded that changes in the A/V ratio are depends both on direction of arteries and veins and on their actual diameter. Based on the results obtained in the star chart method it can also be concluded that for estimating the A/V ratio parallel arteries and veins must be chosen as mentioned in the study [49]. In the study [49] it is recommended to choose parallel segments of the main arteries and veins for estimating the A/V ratio.In other study [50] it is noted that branches of the arteries and veins used for estimating the A/V ratio must be of one and the same division order whereas it is not noted that these branches must be parallel. If unparallel arteries and veins are used for estimating the A/V ratio the estimated A/V ratio is affected by the orientation effect. Special attention to interpretation of the results of ophthalmoscopy must be paid when examining the fundus of eyes suffering from keratoconus. One must also take into account that higher-order ocular aberrations increase due to vapouring of the tear film because during the ophthalmoscopy procedure a patient blinks an eye seldom.

Simulation of aberrations in the star chart and in the retinal image confirms that various aberration patterns influence the diameter of blood vessels differently and hence the A/V ratio. The A/V ratio can be influenced significantly not only aberrations characteristic to keratoconic eyes but also aberrations found in humans which have supernormal vision. The changes in the A/V ratio similar to those observed because of the aberrations are clinically significant and thus it is not known whether the A/V ratio is too large or too small because of some pathology or the optical quality of an eye. Not only the A/V ratio can be under- or overestimated but also too broad or too narrow blood vessels can appear normal. One of the first signs of hypertension is narrowing of retinal arterioles because of elevated blood pressure [51]. Narrowing of retinal arterioles are often classified depending on the A/V ratio [52]. If the A/V ratio is larger than 1/2 then narrowing is classified as belonging to the class I (ranging from small to medium). If the A/V ratio is less than 1/2 then narrowing is classified as belonging to the class II (randing from medium to severe).

The changes in systolic pressure are related to the changes in the A/V ratio [53]. The authors of the study [53] revealed that as large change as 10 mm

Hg in systolic blood pressure causes a 0.02 large change in the A/V ratio. The changes in the A/V ratio because of oscillations in systolic blood pressure can be missed because of ocular aberrations. Narrowing of retinal arterioles is related to hypertension and the risk of diabetes [54]. The authors of the study [54] revealed that patients with lower A/V ratio are at higher risk to get diabetes. Patients who got diabetes the A/V ratio was 0.69 whereas those who didn't get diabetes the A/V ratio was 0.73 the difference being only 0.04.

The A/V ratio is also influenced by pathologies of the optic disc and papilledema [55]. Two most common pathologies of the optic disc are anterior ischemic optic neuropathy and optical neuritis. In both cases patient's complaints are similar and it is difficult to separate these pathologies. The authors of the study [56] revealed that the A/V ratio was equal to 1/3 for 40 % of the whole group with anterior ischemic optic neuropathy while only 8 % of the whole group with optical neuritis had such A/V ratio. Ocular aberrations may impose difficulties when trying to separate these pathologies.

It is unlikely that ophthalmologists when examining the fundus of an eye by using direct or indirect ophthalmoscopy pay attention to patient's and her/his own ocular aberrations and their amount and influence of these aberrations on the A/V ratio. Ophthalmologists use a coarse scale with a large step for estimating the A/V ratio. If such a coarse scale is used the changes in the A/V ratio as large as some hundredths are missed. Fully automatic and semiautomatic software that analyses retinal images and evaluates the A/V ratio used the intensity profile of retinal blood vessels. As software is capable of calculating the A/V ratio with precision several hundredths this software must have tool to correct these aberration effects.

3.5. Design of wavefront correctors

3.5.1. Introduction

In adaptive optics the most frequently used wavefront correctors are deformable mirrors and spatial light modulators. Studies on visual perception using wavefront modulators are mostly performed while the subject is sitting at an optical table onto which a complex optical system has been built. In vision science there are studies related to design of wavefront modulators which could be used in daily life. Intraocular lenses are seen as the most likely candidates for steady correction of ocular higher-order aberrations [57, 58]. Several authors [59, 60, 61] have designed wavefront correctors which could be used similarly to the tradition refractive correction means, i.e., glasses and contact lenses. Wavefront correctors have been designed also in a photoresistive layer [60]. The authors of the study [59] achieved 80 % correction level of ocular higher-order aberrations. Wavefront correctors have been designed also in a PMMA material [60] by using the lathing technology. The authors of the study [61] achieved not only a high level of correction of ocular higher-order aberrations but also significant improvement in visual acuity.

In the doctoral work wavefront correctors were manufactured in a photoresistive layer using a binary grayscale phase mask and their structure and optical properties were evaluated using different methods. The binary grayscale mask is the simplest mask used in lithography. The most popular method for evaluating the wavefront correctors is Shack-Hartmann aberrometry. In the doctoral work aberrometry is compared to profilometry and scanning electron microscopy. The advantage of the last two mentioned methods is considerably higher resolution compared to Shack-Hartmann aberrometry.

3.5.2. The experimental part

3.5.2.1. The optical setup

For measuring and correcting aberrations the optical setup shown in Figure 3.5.2.1.1. was used. Aberrations of the optical setup was measured and corrected at the wavelength λ = 670 nm emitted by a solid state RGB laser. A laser beam was focused on one end of a single mode polarization-maintaining fiber by means of the lens L1 whereas the other end of the fiber was placed in the focal plane of the lens L2. The beam was expanded using a Badal system which was also used to correct defocus. After passing through the Badal system the beam was directed towards the deformable mirror. After being reflected from the deformable mirror the beam was directed into the Shack-Hartmann wavefront sensor. The data acquired by the Shack-Hartmann wavefront sensor was sent to the computer that controlled the shape of the deformable mirror through the control units. This correction mode is called a closed-loop, and it is depicted by the dotted line.

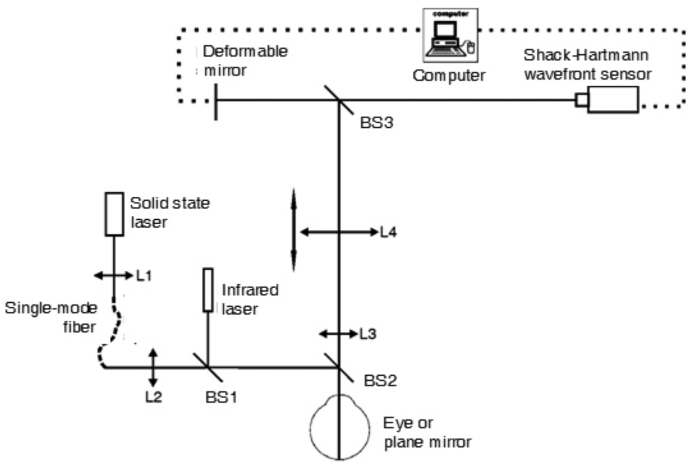

Figure 3.5.2.1.1. The optical setup for measuring aberrations. The optical setup has been described in details in the text. L – lens; BS – beam-splitter.

3.5.2.2. Measurement and correction of aberrations

Aberrations of the optical setup were measured and corrected 5 times. From all measurements the average values of the voltages applied to the electrodes were calculated. These average voltages were applied to the electrodes so that the deformable mirror took the shape needed to compensate aberrations of the optical setup. Next, the residual aberrations of the optical setup were measured 5 times. From all measurements the average values and the standard error was calculated. There was a delay between each two adjacent measurements.

The sum of the subjects' VK and LE aberrations of the right eye and the residual aberrations of the optical setup were measured 5 times. From all measurements the average values and the standard error was calculated. The sum of the subjects' VK and LE aberrations of the right eye and the residual aberrations of the optical setup were measured at the wavelength $\lambda = 850$ nm emitted by an infrared laser. In order to calculate ocular aberrations, the residual aberrations of the optical setup were subtracted from the sum of the aberrations.

3.5.2.3. Design of a phase mask

The wavefronts were generated from Zernike coefficients of the third and fourth order ocular aberrations in Matlab 2007Rb (*Mathworks*). The inverse wavefronts were converted to a grayscale bitmap files encoding the phase of the inverse wavefronts. The phase masks were designed by printing the bitmap files on a transparent film. The phase masks were circles with diameter 5 mm. The binary grayscale phase masks for both subjects VK and LE are shown in Figure 3.5.2.3.1. (a) and (b). In Figure 3.5.2.3.1. (c) the image of the binary grayscale phase mask is shown. The image was acquired by attaching a CCD camera to a light microscope. An area with variable transmittance and periodic holes with no toner can be distinguished. Distance between the holes with no toner was about 180 μm. Diameter of the holes was about 100 μm.

3.5.2.4. Design of the wavefront correctors

3.5.2.4.1. Applying the photoresist to a substrate

The photoresist layer was applied to a microscope slide using the dip-coating method. The slide was immersed into a tank filled up with the photoresist AZ-1350-H (*Shipley*). Next, the slide was pulled out of the tank with speed about 1 mm/s and dried 30 minutes in room temperature. When the photoresist layer had dried the slide was heated in +90°C for 1 minute. This stage is called a prebake.

3.5.2.4.2. Exposure

After prebake the phase mask was superimposed on the slide. The source of UVB radiation was 250 W mercury vapour high-pressure lamp (*Osram*). Distance between the photoresist layer and the lamp was 10 cm. The length of exposure was 1 minute and 30 seconds.

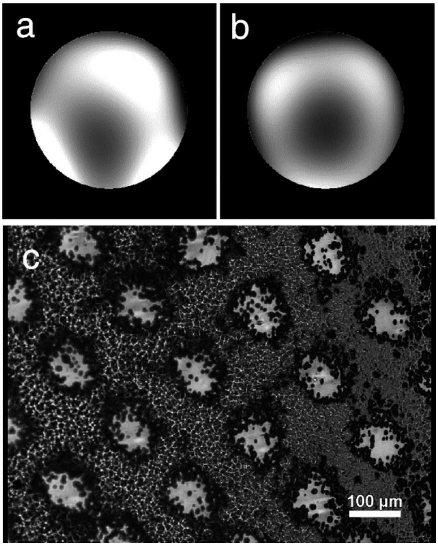

Figure 3.5.2.3.1. The subjects' VK (a) and LE (b) phase masks. In panel (c) an image of a binary grayscale phase mask acquired with a light microscope with a CCD camera attached to it.

3.5.2.4.3. Developing

The photoresist layer was developed in 2.38 % tetramethylammonium hydroxide (molecular formula $C_4H_{13}NO$; abbreviation TMAH; manufacturer Sigma-Aldrich company, Switzerland) solution. As the vapour of TMAH is poisonous, a ducted exhaust hood pulled vapour away. The developing stage lasted 30 seconds and was carried out in room temperature. After developing the slide was postbaked in +120°C for 1 minute.

3.5.2.5. Evaluation of the surface profile

3.5.2.5.1. Aberrometry

For evaluating the wavefront correctors with the aberrometry method the optical setup shown in Figure 3.5.2.1.1. was used. A plane mirror was placed where the subjects' right eye was located previously. First, the aberrations of the unexposed photoresist summed with the residual aberrations were measured. The residual aberrations were subtracted from the measured total aberrations to calculate aberrations of the unexposed photoresist. Next, the aberrations of the wavefront correctors summed with the residual aberrations were measured. The residual aberrations and the aberrations of the unexposed photoresist were subtracted from the total aberrationsto calculate the aberrations of the wavefront correctors.

3.5.2.5.2. Scanning electron microscopy

For evaluating the wavefront correctors with scanning electron microscopy the scanning electron microscope model Zeiss EVO 50 was used. The images were acquired by applying an accelerating voltage U = 5 kV. Prior to applying the scanning electron microscopy method a 5 – 10 nm gold/palladium (Au/Pd) layer was coated on the surface of the wavefront correctors. The slide was frozen in liquid nitrogen and a groove coinciding with the vertical diameter of the wavefront correctors was cut. After the slide and the photoresist layer were frozen it became brittle so that it could be broken easily and viewed from side.

3.5.2.5.3. Profilometry

For evaluating the wavefront correctors the profilometer (a model DekTak D150) was used. The wavefront correctors were scanned along the vertical diameter with a 12.5 μm stylus. Scanning one line took 60 seconds. The coordinates and depth of the surface was saved in ASCII format. Large variations in surface depth because of dust particles adhered to the wavefront correctors were filtered out.

3.5.3. Results

3.5.3.1. Aberrometry

In Figure 3.5.3.1.1. wavefronts of the third and fourth order ocular aberrations for subjects VK and LE are shown. Zernike coefficients have been calculated for a 5 mm pupil. The OSA Zernike polynomial standard was used for describing wavefront aberrations.

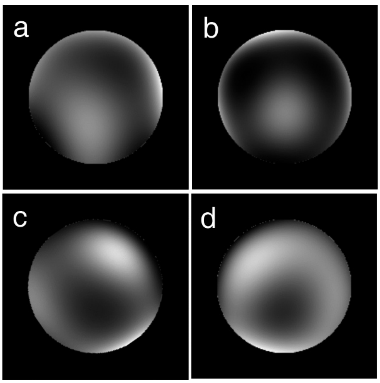

Figure 3.5.3.1.1. The subjects' VK (a) and LE (b) ocular wavefront. The wavefronts of corresponding correctors are shown in panels (c) and (d).

Although the wavefront correctors strongly scattered light the spots formed on the sensing element of the Shack-Hartmann wavefront sensor was sharp and the shape of the wavefront could be reconstructed. When ocular wavefronts are compared to the wavefronts of corresponding wavefront correctors it can be seen that in each point the sign of deformations of both wavefronts is opposite. Although Zernike coefficients of aberrations of the wavefront correctors are considerably smaller than those of higher-order ocular aberrations the shape of the wavefront needed to correct ocular higher-order aberrations is still obtained.

The RMS values of the third and fourth order ocular aberrations are as follow: 0.239 μm (VK) and 0.108 μm (LE).When Zernike coefficients of ocular aberrations are summed with those of aberrations of the wavefront correctors the corresponding RMS value was reduced to 0.206 μm and 0.07 μm, respectively.

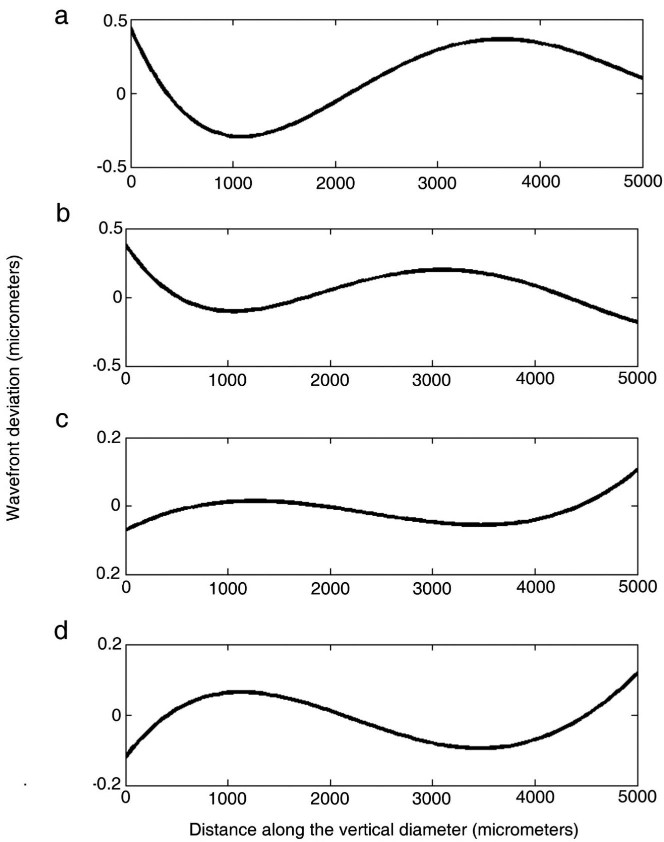

Figure 3.5.3.1.2. Cross-sections of the ocular wavefronts of the third and the fourth order aberrations and the wavefronts of correctors. (a) – the cross-section of the subject's VK ocular wavefront; (b) – the cross-section of the subject's LE ocular wavefront; (c) and (d) – cross-sections of the wavefronts of the corresponding correctors.

A one pixel wide slice was cut out from the wavefronts along their vertical diameter and the profile of the section was obtained (see Figure 3.5.3.1.2.). It can be seen that the deviations of the ocular wavefronts and those of the wavefront correctors are mirror images. In addition, the deviations of the wavefronts of the correctors are much smaller than those of the ocular wavefronts. The cross-sections of the ocular wavefronts are approximately negative multiples of the corresponding cross-sections of the wavefronts of the correctors. In order to assess applicability of the wavefront correctors for correcting ocular aberrations the RMS values of the wavefronts obtained by summing the ocular wavefront and multiples of the wavefronts of the correctors were calculated (see Table 3.5.3.1.2.).

Table 3.5.3.1.2. The RMS for the wavefronts obtained by summing the ocular wavefronts and multiples of the wavefronts of the correctors.

	The RMS (μm)	
	The subject	
Multiple	VK	LE
0	0.239	0.108
1	0.216	0.070
2	0.199	0.056
3	0.189	0.080
4	0.189	0.121
5	0.197	0.168

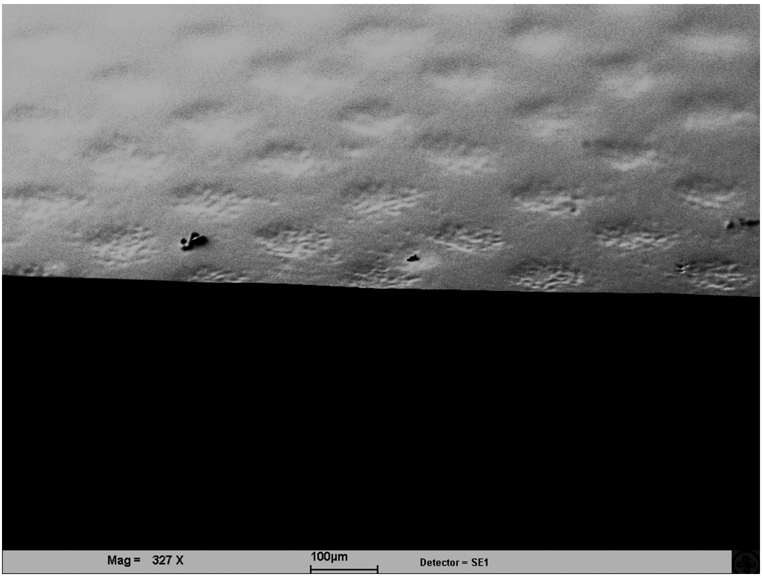

Figure 3.5.3.2.1. The surface of the photoresist after devloping. The even surface was covered by the toner during exposure whereas the wrinkles were formed where there was no toner. The size of the wrinkles is about 10 μm.

3.5.3.2. Scanning electron microscopy

In Figure 3.5.3.2. the surface of the photoresist layer after developing is shown. The size of an individual wrinkle is about 10 µm resulting in strong Mie light scattering. The total area of wrinkles is considerable when compared to to the total area of the wavefront correctors. The diameter of the circles with wrinkles is about 100 µm.

3.5.3.3. Profilometry

In Figure 3.5.3.3.1. it can be seen that the depth of the photoresist surface varies rapidly. The valleys in Figure 3.5.3.3.1. correspond to the circles with the wrinkles.

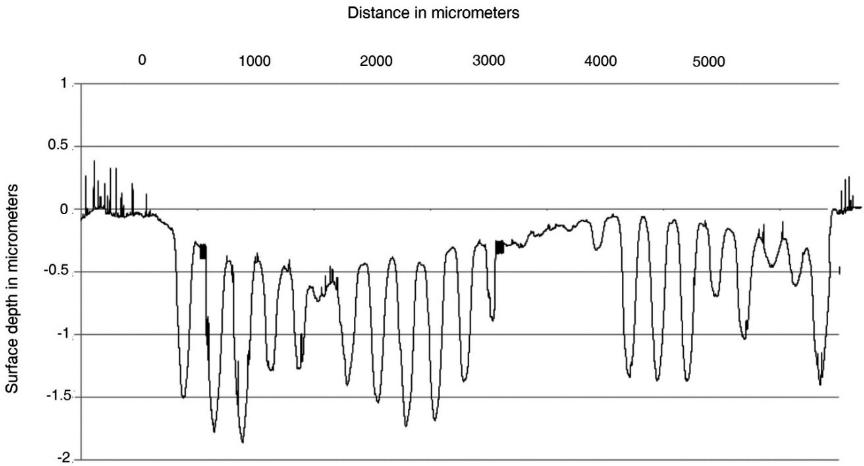

Figure 3.5.3.3.1. Changes in the depth of the surface of the wavefront correctors along the diameter (subject VK). The correctors were scanned along the vertical diameter. The length of one scan is 5 mm.

3.5.4. Analysis

The shape of the wavefront of the correctors is that required for successful compensation of ocular aberrations. This is confirmed by the ocular wavefront map and the wavefront map of the correctors. The correct shape of the wavefront correctors is also confirmed by the cross-sections of the wavefronts. However, although the measured Zernike coefficients are comparable to the average values measured in a large population [48] these are too small to compensate for the measured ocular aberrations. The cross-sections of the ocular wavefronts (see Figure 5) are as large as those of envelopes fitted to the data of the profilometer. This raises a question why the absolute values of Zernike coefficients of the wavefront of the wavefront correctors are much smaller than those of the ocular wavefronts. This contradiction may be explained by that the real surface profile isn't even but rapidly varies in depth along the diameter of the wavefront correctors. Another way how to acquire a uniform change in light intensity and the depth of the surface is to use reduction optics commonly used in optical lithography to compress image a large phase mask on a photoresist layer. The photoreduction process has been described in the study [60], however, details are not given.

As seen in Results section by adding multiples of the wavefront of the wavefront correctors to the ocular wavefront resulted in decreased RMS value. The reason why the maximal reduction in the RMS value was about 0.05 μm may be differences between alignment of the eye with the optical axis and that of the wavefront correctors. Navarro [60] also pointed to the role of extremely precise alignment of the wavefront corrector and the eye for successful correction of ocular aberrations.

The use of a binary amplitude mask is also limited by the diffraction of light. Although the spots of the Shack-Hartmann wavefront sensor were easy visible the performance of the wavefront correctors was impaired by considerable level of light scattering. As light scattering is one of the factors strongly influencing visual perception it must be minimized as much as possible. It can be concluded that light scattering is caused by the wrinkles seen in the images acquired with the scanning laser ophthalmoscopy method. The wrinkles originate from near-field diffraction in the holes where there is no toner. The structure of the wrinkles is similar to distribution of light intensity when light diffracts in a rectangular aperture. Depending on the local light intensity variable amount of the photoresist layer is wiped away during developing. The total area of wrinkles is considerable compared to the total area of the wavefront correctors.

Although increasing the distance between the binary amplitude mask and the photoresistive layer may reduce large depth variations of the surface it must be noted that if there is a space between the mask and the photoresistive layer diffraction effects and therefore light scattering may actually be increased. It is known that proximity lithography is limited by light diffraction [62]. Using a halogen lamp for illuminating the photoresist may decrease the light scattering effects. The coherence length of mercury lines are several tens of micrometers [63] whereas it is less than one micrometer in a case of tungsten halogen lamp [64].

The wavefront modulators designed by using a binary amplitude mask could be used as calibration plates like in the study carried out by Rodríguez et al. [65]. Rodríguez et al. measured the amount of aberrations with the Shack-Hartmann wavefront sensor and Mach-Zehnder interferometer and after applied them to calibrate laser ray tracing aberrometer. In this application of the wavefront modulators the light scattering isn't important unless the centroids of the Shack-Hartmann spots can be easily calculated and an interferogram can be generated.

3.6. Influence of calibration parameters on measurements of aberrations

3.6.1. Introduction

Adaptive optics requires to define a referent state or a plane wavefront. This definition is a bitmap file containing information about location of Shack-Hartmann spots. Further in the text the bitmap file containing information about location of the spots will be called a reference. Ideally, distance between any two neighbouring Shack-Hartmann spots is one and the same and this distance is equal to that between centers of two neighbouring lenslets corresponding to a certain distance in pixels. The manufacturing process of a Shack-Hartmann wavefront sensor isn't ideal. A consequence of these imperfections is asymmetric placement of the lenslets. Because of imperfections in the manufacturing process an ideal reference is that acquired as a plane wavefront enters a Shack-Hartmann wavefront sensor.

Little information regarding the way how the reference must be set is available in literature. In the study [66] a spherical wavefront was used for calibration of a Shack-Hartmann wavefront sensor. A source of the spherical wavefront was an end of a single-mode polarization maintaining fiber. The use of the fiber ensures an extremely small amount of aberrations in the spherical wavefront. At distance several meters away from the end of the fiber curvature of the wavefront becomes small and thus it is possible to obtain a reference that is close to the ideal one. As mentioned in the study [67] the reference can be obtained either by using a spherical wavefront as described in the study [66] or a plane wavefront obtained when a point source is placed in the focal plane of the paraxial region of a lens.

In the doctoral work the reference was set both using a spherical and an aspheric lens. The aim of the study was to assess the systematic error of aberration measurements caused by different spot patterns in the references.

3.6.2. The experimental part

3.6.2.1. Subjects

Six subjects were enrolled in the experiment. The refractive error of the subjects' right eye is shown in Table 3.6.2.1.1. None of the subjects had any pathologies of the visual system.

Table 3.6.2.1.1. The subjects' refractive error.

The subject	Sphere	Cylinder
VK	-0.50 D	-0.50 D
GK	-5.00 D	-0.75 D
KL	+0.50 D	0.00 D
JS	-3.75 D	0.00 D
LE	+0.50 D	+0.25 D
MD	-2.00 D	-1.50 D

3.6.2.2. Calibration of the Shack-Hartmann wavefront sensor

In the experiment an optical system similar to that used in the study [67] was used. The optical setup is shown in Figure 3.6.2.2.1. A laser beam (a wavelength λ = 670 nm) was focused on an end of a single-mode polarization maintaining fiber by using the lens L1. The outgoing beam was collimated by placing the other end of the fber in the focal plane of the lens L2. The beam was collimated both when using an aspheric lens and when using a spherical lens.

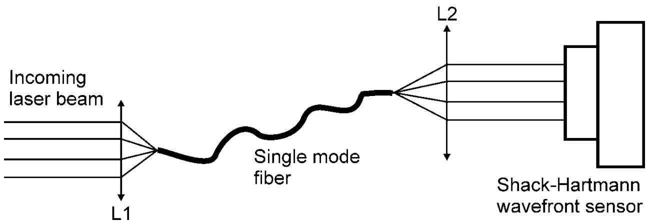

Figure 3.6.2.2.1. Setting the reference in adaptive optics. A laser beam is focused on one end of a single-mode fiber whereas the other end is placed in the focal plane of either a spherical or an aspheric lens. When a collimated beam enters into the Shack-Hartmann wavefront sensor the reference is set. L – lens.

When the spherical lens was used for calibration purposes the end of the fiber was placed in the focal plane of the paraxial focus. The beam was collimated by placing the end of the fiber at such a distance from the lens that the diameter of the beam was one and the same both close to the lens and several meters away from it. When the beam was collimated the reference was set.

3.6.2.3. Measurement of aberrations

Aberrations were measured in two stages. The OSA Zernike polynomial standard was used for describing the wavefronts. In the first stage the total of aberrations of the optical setup and ocular aberrations was measured. Measurements were done by using the optical setup shown schematically in Figure 3.6.2.4.1. The sum of aberrations was measred at the wavelength λ = 850 nm emitted by an infrared laser. The Badal system consisting of the lenses L1 and L2 was used to correct defocus and expand a pupil of an eye to the entrance pupil of the Shack-Hartmann wavefront sensor. The lenses L1 and L2 were placed so that defocus was 0 D when measured against the aspheric reference. There was a several minutes long pause between two sequential measurements.

In the next stage the aberrations of the optical setup were measured. The aberrations of the optical system were measured at the wavelength λ = 670 nm emitted by a solid state RGB laser when a collimated beam was reflected by a plane mirror. There was a several minutes long pause between two sequential measurements. In order to calculate ocular aberrations, the aberrations of the optical setup were subtracted from the total aberrations.

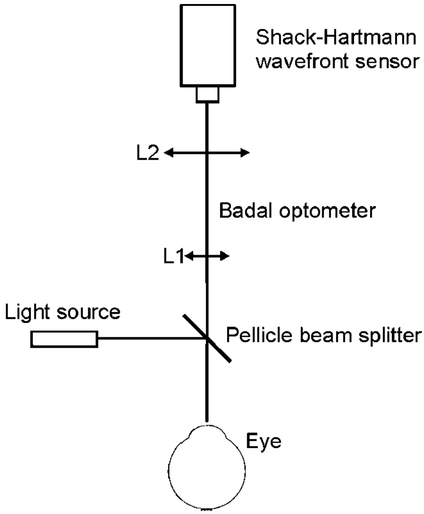

Figure 3.6.2.4.1. The optical setup for measuring aberrations. The optical setup has been described in details in the text. L – lens.

3.6.3. Results

3.6.3.1. Shifts of centroids

The deviations of the centroids in the central and the peripheral regions of the pixel array are shown in Figure 3.6.3.1.1. A and B. The red columns correspond to the reference set with the aspheric lens while the green columns are shown for the spherical case.

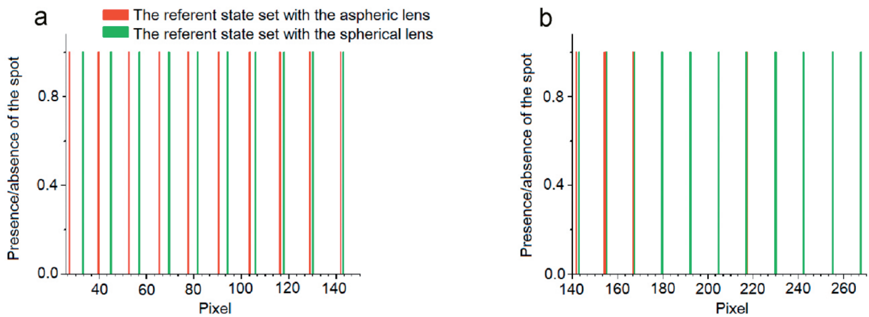

Figure 3.6.3.1.1. Referent spot positions obtained by using the spherical (green bars) and the aspheric (red bars) collimating lens. Panel A shows the peripheral region of the lens while the Panel B shows the central region. Spot positions have been calculated by centroiding algorithms. In the center of the spot pattern (around pixel coordinate 260) spot positions in both cases overlap whereas towards the periphery the sphericity of the spherical lens causes the referent positions to deviate away.

It can be seen in Figure 3A and 3B that in the central regions centroids calculated for the spherical and the aspheric reference coincide with each other whereas in a far peripheral region of the pixel array the centroids has been displaced by 4.9 pixels equal to 4.9·P = 57.58 μm because of the spherical aberration. From Eq. (4) the slope and the radius of curvature of the wavefront incident on the lenslet array R ≈ 0.163 m can be calculated. This corresponds to the optical power +6.1 D.

The spherical aberration of the lens was calculated by using freely available OSLO software intended for various simulation tasks in optics. The entrance pupil of the SHWS is 36 mm and that's why the longitudinal spherical aberration at distance 18 mm from the optic axis was calculated. By choosing the appropriate values of curvature of the surfaces, the focal length and the diameter of the lens the value of the longitudinal spherical aberration 3 mm was obtained. This corresponds to a change in optical power 0.15 D when compared to the paraxial region.

Relay lenses with the focal length 240 mm and 40 mm and magnification M = 6 are placed in the front of the lenslet array. The curvature of the wavefront incident on the lenslet array is calculated by using the basic lens equation

$$\frac{1}{l\prime} = \frac{1}{l} + F \qquad (3.6.3.1.1.)$$

where l' is the distance of the image from the lens, l is the distance of the object from the lens, but F is the optical power of the lens.

Now, by applying the lens Eq. (5) again it can be calculated that the curvature of the wavefront incident on the lenslet array is about 207 mm corresponding to the optical power +4.82 D. This is close to the value calculated from the displacements of the centroids. Thus it can be concluded that 0.15 D is a reasonable estimate of the spherical aberration of the lens used for setting the referent state.

3.6.3.2. Measurements of ocular aberrations

Next, results of the measurements of ocular aberrations are given. The measured Zernike coefficients for each subject are shown in Figure 3.6.3.2.1. Piston and tip/tilt are excluded since these aberrations don't change the shape of the wavefront. Zernike coefficients up to 6^{th} order have been shown.

Table 3.6.3.2.1. The total RMS, LOA RMS, and HOA RMS in the case of the aspheric and the spherical reference.

	Total RMS (μm)		LOA RMS (μm)		HOA RMS (μm)		Pupil size (mm)
The subject	Asph	Sph	Asph	Sph	Asph	Sph	
VK	0.431	0.488	0.415	0.472	0.114	0.123	5.5
GK	1.578	0.601	1.536	0.522	0.363	0.299	5.2
KL	0.596	0.387	0.583	0.290	0.123	0.080	5.2
JS	1.279	0.952	1.252	0.931	0.258	0.196	4.5
LE	0.501	0.369	0.487	0.346	0.115	0.128	4.7
MD	1.045	0.652	1.028	0.635	0.190	0.148	4.7

As expected the LOA had the largest magnitude and also demonstrated the largest dependence on the type of the reference. Among HOA spherical aberration c_4^0 had the largest magnitude measured against either reference. In Table 3.6.3.2.1. the total RMS, the LOA RMS and the HOA RMS has been summarized for each subject. Among HOA the magnitude of coma and spherical aberration was influenced the most by the type of the referent state.

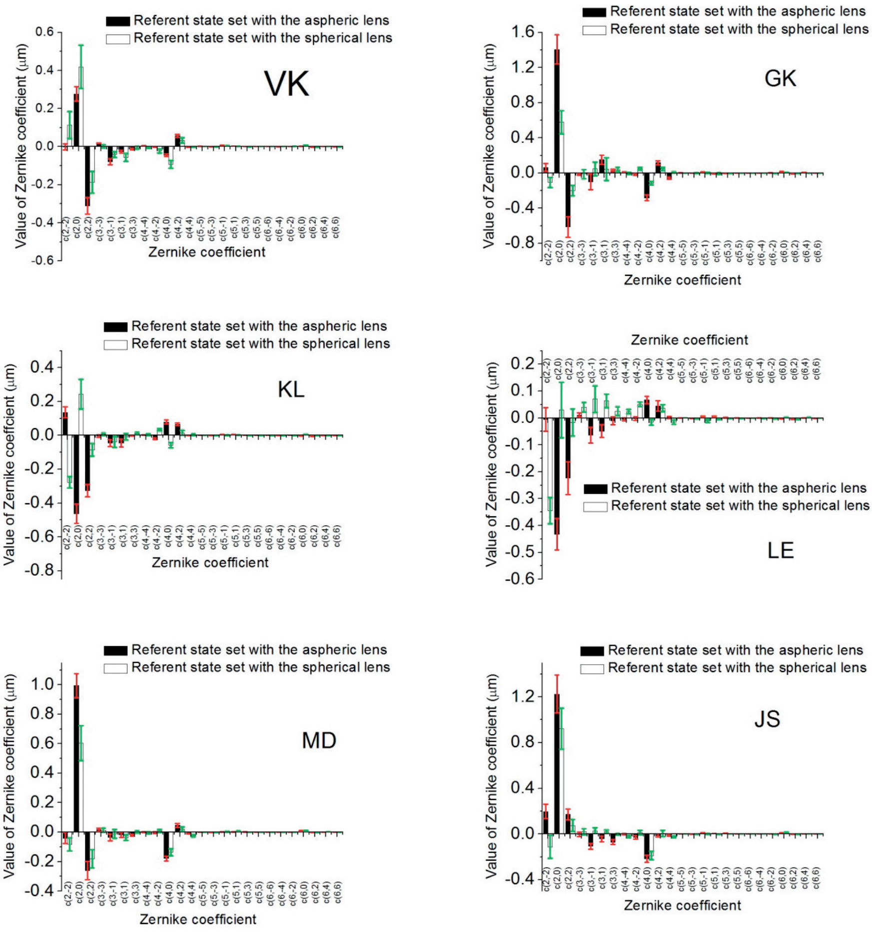

Figure 3.6.3.2.1. Measured Zernike coefficients for all subjects (identified by the initials) and measured against both references. Black columns show aberrations measured against the aspheric reference, white columns are shown for the spherical reference. Piston and tip/tilt are excluded. Zernike coefficients up to 6th order have been shown. The error bars shown are standard errors calculated from 5 measurements.

In general, both the total RMS and LOA RMS, and HOA RMS were smaller when measured against the spherical reference compared to the aspheric reference. LOA contributed the most in reduction of total RMS when measuring aberrations against the spherical reference. HOA RMS changed by only some hundredths of µm.

3.6.4. Analysis

First of all the data obtained when the aspheric reference was used are analyzed. The subjects' LE, KL and VKrefractive error corresponds well to optical power vectors M, J_o and J_{45}. Subjects KL and LE have small positive spherical aberration whereas the subject VK had small negative spherical aberration. The amount and sign of all three subjects' spherical aberration is in agreement with studies in which development of aberrations throughtout the life has been analyzed. Emmetropic and hypermetropic subjects have positive spherical aberration and it increases with age. Negative spherical aberration is characteristic to a myopic population.

The optical power vectors correspond well to the subjects' JS and MD refractive error whereas inconsistency is observable for the subject GK (see Table 3.7.3.2.1.). A possible cause of the inconsistency is the large refractive error. A large refractive error cause large deviations of the spots resulting in assignment of spots to the wrong lenslets. This is called a wrapping effect [68]. All three subjects have negative spherical aberration that initially may seem contrary to changes in spherical aberration with age, i.e., spherical aberrations becomes more positive. However, there are studies the results of which confirm that myopic subjects have negative spherical aberration [69, 70].

Further in the text the measurements measured against the spherical reference are analyzed. Similarly to the case of the aspheric reference the amount of lower order aberration exceed that of other aberrations and the amount of spherical aberration exceeds that of other higher order aberrations. Generally, both the total RMS, and the RMS of the lower-order aberrations and the RMS of the higher-oorder aberrations were smaller when aberrations were measured against the spherical reference (see Table 3.7.3.2.1.). The amount of spherical aberration measured in the subjects KL and LE was reduced. The reducded amount of spherical aberration may be explained by spherical aberration in the reference. A reduction in the amount of defocus and in spherical aberration was observed for the subject VK. A reduction in the amount of defocus was observed for the subjcts GK, JS and MD. The optical power vectors calculated from the Zernike coefficients measured against the spherical reference have been summarized in Table 3.7.3.2.1. In the case of a small myopia/hypermetropia the opposite type of ametropia can be measured. A moderate myopia (subjects JS and MD) can be underestimated. For the subject GK inconsistiency between the optical power vectors and the refractive error was larger compared to that in the case of the aspheric reference. It can be concluded that a spherical reference limits the dynamic range of a Shack-Hartmann wavefront sensor in a similar way like the wrapping effect. In addition, these effects can sum together.

The results obtained show that the measured amount of aberrations depends on the reference used. As could be expected the change of the reference influenced the measured amount of the lower-order aberrations more than that of the higher-order aberrations. Several authors have analyzed the distribution of Zernike coefficients in a large population.The amount of aberrations differs not only when measured with different methods but also when using different Shack-Hartmann wavefront sensors [71]. In the study [71] four different wavefront sensors were compared. Two of these wavefront sensors (Irx3 and Keratron) are based on the Shack-Hartmann principle. The aberrations were measured for a pupil size 5 mm. The difference between the amounts of defocus c_2^0 measured by the Irx3 and the Keratron was 0.92 μm corresponding approximately to 1 D. There was not only a difference between the amounts of defocus but also between the amounts of spherical aberration and trefoil. In the study carried out in the doctoral work it can be concluded that the reason of the differences between measured amounts of different aberrations are different procedures used to calibrate wavefront sensors.

In the study [72] a Bausch and Lomb Zywave Shack-Hartmann wavefront sensor was compared to an autorefractometer. For a pupil size 5 mm a 0.3 D large difference between defocus was found. This difference corresponds to difference 0.3 μm between the values of the coefficient c_2^0. In the study [73] wavefront aberrometers WaveScan, LADARWave and Zywave were compared. All these three wavefront aberrometers are based on the Shack-Hartmann principle. In the study [73] a difference in the RMS value of higher-order aberrations 0.2 μm was obtained.

In the study [48] wavefront aberrations up to 6^{th} in a large emmetropic population were measured by using a wavefront sensor Allegreto. The authors of the study [48] observed a small amount of the positive spherical aberration (+0.08 μm for a pupil size 6 mm). In other studies [74, 75] a considerably larger value of spherical aberration was obtained. It is known that spherical aberration increases in the positive direction with age. As a possible source of the observed difference the authors of the study [48] suggested the internal positive spherical aberration of the aberrometer. This internal positive spherical aberration reduces the negative ocular spherical aberration. In a similar way the results obtained in the doctoral work are explained.

The choice of the reference can also influence correction of aberration with adaptive optics. The measured amount of aberrations corresponds better to the objective refraction and to the results obtained in other studies if the reference is set with the aspheric lens. If the reference is set with a spherical lens then adaptive optics doesn't correct the aberrations fully.

Practical significance

1. The results obtained in the doctoral work allow to analyze how significant are the optical defects of an eye in daily life. Acquired knowledges about the adaptation processes indicate to what extent ocular aberrations must be corrected. Studies of Vernier acuity confirm that the visual system makes use of the blur caused by aberrations, i.e., the blur is the physiological basis of specific visual functions.
2. Simulation of aberrations prove that when using a software that automatically analyzes retinal images the aberration effects must be taken into account. If an ophthalmologist has an aberrometer the retinal images can be processed mathematically thus neutralizing the aberration effects and their influence on appearance of retinal structures.
3. For precise measurements/correction of aberrations careful calibration of adaptive optics is necessary. For calibration purposes phase plates with a certain aberration pattern and optical power are often used. In the doctoral work it has been shown that such phase plates can be manufactured using a very simple binary grayscale mask and advanced lithography methods are not required.

References

1. L. Zhu, P. C. Sun, D. U. Bartsch, W. R. Freeman, Y. Fainman. „Wave-front generation of Zernike polynomial modes with a micromachined membrane deformable mirror". Applied Optics 38, 6019 – 6026 (1999).
2. E. Hecht. Optics (4th edition). Pearson Addison Wesley, 539 (2003).
3. X. Cheng, A. Bradley, S. Ravikumar, L.N. Thibos. „The visual impact of Zernike and Seidel forms of monochromatic aberrations". Optometry & Vision Science 87, 300 – 312 (2010).
4. S. Marcos, L. Sawides, E. Gambra, C. Dorronsoro. „Influence of adaptive-optics ocular aberration correction on visual acuity at different luminances and contrast polarities". Journal of Vision 13, 1–12 (2008).
5. J. Liang, D. R. Williams, D. T. Miller. „Supernormal vision and high-resolution retinal imaging through adaptive optics". Journal of the Optical Society of America A 14, 2884 – 2892 (1997).
6. N. Yamane, K. Miyata, T. Samejima, T. Hiraoka, T. Kiuchi, F. Okamoto, Y. Hiro-hara, T. Mihashi, T. Oshika. „Ocular higher-order aberrations and contrast sensitivity after conventional laser in situ keratomileusis". Investigative Ophthalmology & Visual Science 45, 3986–3990 (2004).
7. J. R. Jiménez, J. J. Castro, R. Jiménez, E. Hita. „Interocular differences in higher-order aberrations on binocular visual performance". Optometry and Vision Science 85, 174 – 179 (2008).
8. L. Chen, P. B. Kruger, H. Hofer, B. Singer, D. R. Williams. „Accommodation with higher-order monochromatic aberrations corrected with adaptive optics". Journal of the Optical Society of America A 23, 1 – 8 (2006).
9. S. Li, Y. Xiong, J. Li, N. Wang, Y. Dai, L. Xue, H. Zhao, W. Jiang, Y. Zhang, J. C. He. „Effects of monochromatic aberration on visual acuity using adaptive optics". Optometry and Vision Science 86, 868 – 874 (2009).
10. P. Artal, L. Chen, E. J. Fernández, B. Singer, S. Manzanera, D. R. Williams. „Neural compensation for the eye's optical aberrations". Journal of Vision 4, 281 – 287 (2004).
11. L. Chen, P. Artal, D. Gutierrez, D. R. Williams. „Neural compensation for the best aberration correction". Journal of Vision 7, 1 – 9 (2007).
12. D. X. Hammer, R. D. Ferguson, C. E. Bigelow, N. V. Iftimia, T. E. Ustun. „Adaptive optics scanning laser ophthalmoscope for stabilized retinal imaging". Optics Express 14, 3354 – 3367 (2006).
13. P. Godara, A. M. Dubis, A. Roorda, J. L. Duncan, J. Carroll. „Adaptive optics retinal imaging: emerging clinical applications". Optometry and Vision Science 87, 930 – 941 (2010).
14. A. Roorda, F. R. Borja, W. Donnelly, H. Queener, T. Hebert, M. Campbell. „Adaptive optics scanning laser ophthalmoscopy". Optics Express 10, 405 – 412 (2002).
15. A. R. Elkington, H. J. Frank, M. J. Greaney. Clinical optics. Wiley-blackwell, 235 (1999).
16. J. J. Hunter, M. C. W. Campbell. „Potential effect on the retinoscopic reflex of scleral Eexpansion surgery for presbyopia". Optometry and Vision Science 83, 649 – 656 (2006).
17. http://www.imagine-eyes.com/content/view/26/51/
18. http://wps.prenhall.com/wps/media/objects/1351/1384175/image/simple_adaptive_optics.gif
19. V. Lakshminarayanan, J. M. Enoch. „Vernier acuity and aging". International Ophthalmology 19, 109 – 115 (1995).
20. M. Ozolinsh, I. Martín, D. Lauva, V. Karitans. „Howard-Dolman stereovision test at different opponent colour stimuli". (pieņemts publicēšanai žurnālā *Journal of Modern Optics*).

21. A. W. Snyder, D. T. Miller. „Photoreceptor diameter and spacing for highest resolving power" Journal of the Optical Society of America A 67, 696 – 697 (1977).
22. G. Westheimer. „The spatial sense of the eye". Investigative Ophthalmology & Visual Science 18, 893 – 912 (1979).
23. R. A. Williams, J. M. Enoch, E. A. Essock. „The resistance of selected hyperacuity configurations to retinal image degradation". Investigative Ophthalmology & Visual Science 25, 389 – 399 (1984).
24. M. H. Hennig, F. Wörgötter. „Eye micro-movements improve stimulus detection beyond the Nyquist limit in the peripheral retina". Advances in Neural Information Processing Systems 16, 1475 – 1482 (2004).
25. A. W. Snyder. „Hyperacuity and interpolation by the visual pathways". Vision Research 22, 1219–1220 (1982).
26. M. Malania, M. H. Herzog, G. Westheimer. „Grouping of contextual elements that affect Vernier thresholds". Journal of Vision 7, 1 – 7 (2007).
27. R. A. Crone, O. M. Leuridan. „Tolerance for aniseikonia. II. Determination based on the amplitude of cyclofusion". Albrecht von Graefes Archiv fur klinische und experimentelle Ophthalmologie 188, 17–22 (1973).
28. M. A. Webster, Y. Mizokami, L. A. Svec, S. L. Elliott. „Neural adjustments to chromatic blur". Spatial Vision 19, 111–132 (2006).
29. J. S. Werner, S. L. Elliott, S. S. Choi, N. Doble. „Spherical aberration yielding optimum visual performance: Evaluation of intraocular lenses using adaptive optics simulation". Journal of Cataract & Refractive Surgery 35, 1229 – 1233 (2009).
30. S. Süsstrunk, J. Holm, G. D. Finlayson. „Chromatic adaptation performance of different RGB sensors". IS&T/SPIE Electronic Imaging 4300, 1 – 12 (2001).
31. J. H. Hateren, H. P. Snippe. „Phototransduction in primate cones and blowfly photoreceptors: different mechanisms, different algorithms, similar response". Journal of Comparative Physiology A 192, 187 – 197 (2006).
32. D. Tranchina, J. Sneyd, I. D. Cadenas. „Light adaptation in turtle cones. Testing and analysis of a model for phototransduction". Biophysical Journal 60, 217 – 237 (1991).
33. G. L. Fain, H.R. Matthews, M. C. Cornwall, Y. Koutalos. „Adaptation in vertebrate photoreceptors". Physiological Reviews 81, 117–151 (2001).
34. C. J. Bartleson. „Changes in color appearance with variations in chromatic adaptation". Color Research & Application 4, 119–138 (2007).
35. D. Alleysson, S. Süsstrunk. „On adaptive non-linearity for color discrimination and chromatic adaptation". Proc IS&T Conf on Color in Graphics, Imaging and Vision 1, 190–195 (2002).
36. J. S. Wang, M. E. Estevez, M. C. Cornwall, V. J. Kefalov. „Intra-retinal visual cycle required for rapid and complete cone dark adaptation". Nature Neuroscience 12, 295–302 (2009).
37. A. Daugirdienė, H. Vaitkevičius. „Colour perception: contrast and adaptation". Biologija 2, 32 – 36 (2002).
38. F. Keller, P. Koeppe, C. Emde. „Exponential function of chymotrypsin action". Enzyme 31, 39–44 (1984).
39. J. B. Hurley. „Shedding light on adaptation". The Journal of General Physiology 119, 125 – 128 (2002).
40. O. Rinner, K. R. Gegenfurtner. „Time course of chromatic adaptation for color appearance and discrimination". Vision Research 40, 1813–1826 (2000).
41. M. D. Fairchild, L. Reniff. „Time course of chromatic adaptation for color appearance judgments". Journal of the Optical Society of America A 12, 824–833 (1995).

42. http://vision.berkeley.edu/roordalab/aoslo.htm
43. A. A. Martinez, P. R. Sankaridurg, T. J. Naduvilath, P. Mitchell. „Monochromatic aberrations in hyperopic and emmetropic children". Journal of Vision 9, 1 – 14 (2009).
44. A. Guirao, M. Redondo, E. Geraghty, P. Piers, S. Norrby, P. Artal. „Corneal optical aberrations and retinal Image quality in patients in whom monofocal intraocular lenses were implanted" Archives of Ophthalmology 120, 1143 – 1151 (2002).
45. R. Kosaki, N. Maeda, K. Bessho, Y. Hori, K. Nishida, A. Suzaki, Y. Hirohara, T. Mihashi, T. Fujikado, Yasuo Tano. „Magnitude and orientation of Zernike terms in patients with keratoconus". Investigative Ophthalmology & Visual Science 48, 3062 – 3068 (2007).
46. Y. Levy, O. Segal, I. Avni, D. Zadok. „Ocular higher-order aberrations in eyes with supernormal vision". American Journal of Ophthalmology 139, 225 – 228 (2005).
47. J. C. He, P. Sun, R. Held, F. Thorn, X. Sun, A. Gwiazda. „Wavefront aberrations in eyes of emmetropic and moderately myopic school children and young adults". Vision Research 42, 1063 – 1070 (2002).
48. S. Plainis, I. G. Pallikaris. "Ocular monochromatic aberration statistics in a large emmetropic population". Journal of Modern Optics 55, 759–772 (2008).
49. C. Muramatsu, Y. Hatanaka, T. Iwase, T. Hara, H. Fujita. „Automated detection and classification of major retinal vessels for determination of diameter ratio of arteries and veins". Proc. of SPIE 7624, 76240J-1 (2010).
50. N. L. Stokoe, R. W. D. Turner. „Normal retinal vascular pattern". British Journal of Ophthalmology 50, 21 – 40 (1966).
51. T. T. Nguyen, J. J. Wang, F. M. A. Islam, P. Mitchell, R. J. Tapp, P. Z. Zimmet, R. Simpson, J. Shaw, T. Y. Wong. „Retinal arteriolar narrowing predicts incidence of diabetes: the australian diabetes, obesity and lifestyle (AusDiab) study". Diabetes 57, 536 – 539 (2007).
52. B. J. H. Born, C. A. A. Hulsman, J. B. L. Hoekstra, R. O. Schlingemann, G. A. Montfrans. „Value of routine funduscopy in patients with hypertension: systematic review". BMJ 331, 1–5 (2005).
53. A. R. Sharrett, L. D. Hubbard, L. S. Cooper, P. D. Sorlie, R. J. Brothers, F. J. Nieto, J. L. Pinsky, R. Klein. „Retinal arteriolar diameters and elevated blood pressure". American Journal of Epidemiology 150, 263 – 270 (1999).
54. T. Y. Wong, A. Shankar, R. Klein, B. E. K. Klein, L. D. Hubbard. „Retinal arteriolar narrowing, hypertension, and subsequent risk of diabetes mellitus". Archives of Internal Medicine 165, 1060 – 1065 (2005).
55. P. Jain, A. Gupta, B. K. Sharma. „A correlative study of ophthalmoscopy and fluorescein angiography in systemic hypertension". Indian Journal of Ophthalmology 38, 169 – 174 (1990).
56. E. Z. Rath, U. Rehany, S. Linn, S. Rumelt. „Correlation between optic disc atrophy and aetiology: anterior ischaemic optic neuropathy vs optic neuritis". Eye 17, 1019 – 1024 (2003).
57. L. Wang, D. D. Koch. „Effect of decentration of wavefront-corrected intraocular lenses on the higher-order aberrations of the eye". Archives of Ophthalmology 123, 1226 – 1230 (2005).
58. R. Bellucci, S. Morselli. „Optimizing higher-order aberrations with intraocular lens technology". Current Opinion in Ophthalmology 18, 67 – 73 (2007).
59. S. Fomins, M. Reinfelde, A. Larichev, N. Iroshnikov, A. Gerbreders, M. Ozolinsh. „Photoinduced AsSeS thin film phase plates as adaptive optics mirrors for eye aberration correction". Proc. SPIE 7142, 71421C (2008).
60. R. Navarro, E. M. Barriuso, S. Bará, and T. Mancebo. „Phase plates for wave-aberration compensation in the human eye". Optics Letters 25, 236 – 238 (2000).

61. G. Yoon, T. M. Jeong, I. G. Cox, D. R. Williams. „Vision improvement by correcting higher-order aberrations with phase plates in normal eyes". Journal of Refractive Surgery 20, 523 – 527 (2004).
62. R. Voelkel, U. Vogler, A. Bich, P. Pernet, K. J. Weible, M. Hornung, R. Zoberbier, E. Cullmann, L. Stuerzebecher, T. Harzendorf, U. D. Zeitner. "Advanced mask aligner lithography: new illumination system". Optics Express 18, 20968 – 20978 (2010).
63. C. Falldorf, W. Osten, E. Kolenovic. „Speckle shearography using a multiband light source". Optics and Lasers in Engineering 40, 543 – 552 (2003).
64. Y. Chen, H. Zhao, Z. Wang. „Investigation on spectral-domain optical coherence tomography using a tungsten halogen lamp as light source". Optical Review 16, 26 – 29 (2009).
65. P. Rodríguez, R. Navarro, J. Arines, S. Bará. „A new calibration set of phase plates for ocular aberrometers". Journal of Refractive Surgery 22, 275 – 284 (2006).
66. A. Chernyshov, U. Sterr, F. Riehle, J. Helmcke, J. Pfund. "Calibration of a Shack–Hartmann sensor for absolute measurements of wavefronts". Applied Optics 44, 6419 – 6425 (2005).
67. G. Artzner. „On the absolute calibration of Shack-Hartmann sensors and UT laboratory wavefront measurements". Pure and Applied Optics 3, 121 – 132 (1994).
68. L. Lundström, P. Unsbo. "Unwrapping Hartmann-Shack images from highly aberrated eyes using an iterative b-spline based extrapolation method". Optometry and Vision Science 81, 383 – 288 (2004).
69. F. Karimian, S. Feizi, A. Doozande. „Higher-order aberrations in myopic eyes". Journal of Ophthalmic and Vision Research 5, 3 – 9 (2010).
70. G. Yoon, S. MacRae, D. R. Williams, I. G. Cox. „Causes of spherical aberration induced by laser refractive surgery". Journal of Cataract & Refractive Surgery 31, 127 – 135 (2005).
71. N. Visser, T. T. Berendshot, F. Verbakel, A. N. Tan, J. Brabander, R. M. Nuijts, "Evaluation of the comparability and repeatability of four wavefront aberrometers". Investigative Ophthalmology & Visual Science 10, 1302 – 1311 (2011).
72. M. J. Dobos, M. D. Twa, M. A. Bullimore. „An evaluation of the Bausch & Lomb Zywave aberrometer". Clinical and Experimental Optometry 92, 238 – 245 (2009).
73. C. L. Liang, S. H. H. Juo, C. J. Chang. „Comparison of higher-order wavefront aberrations with 3 aberrometers". Journal of Cataract & Refractive Surgery 31, 2153 – 2156 (2005).
74. J. Bao, R. Le, J. Wu, Y. Shen, F. Lu, J. C. He. „Higher-order wavefront aberrations for populations of young emmetropes and myopes". Journal of Optometry 2, 51 – 58 (2009).
75. J. F. C. Mochón, N. L. Gil, A. Benito, P. Artal P. „Ocular wave-front aberration statistics in a normal young population". Vision Research 42, 1611 – 1617 (2002).

List of publications

1. M. Ozolinsh, M. Colomb, G. Ikaunieks, V. Karitans. "Color stimuli perception in presence of light scattering". Visual Neuroscience, 23, 597-601 (2006).
2. V. Karitans, M. Ozolinsh, G. Kuprisha. "Electronic eye occluder with time-counting and reflection control". Proc. SPIE 7142, 71421B-71421B-8 (2008).
3. S. Fomins, M. Ozolinsh, G. Krumina, V. Karitans. „Ferroelectric Liquid Crystal Glasses For Amblyopia Research" Integrated Ferroelectrics 103, 10 – 18 (2008).
4. V. Karitans, M. Ozolinsh. „Method for compensation of eye movements in adaptive optics". Latvian Journal of Physics and Technical Sciences 47, 51 – 56 (2010).
5. M. Kuibida, V. Karitans. „Influence of optical aberrations of an eye on resolution of dichoptic images". Latvian Journal of Physics and Technical Sciences 47, 55 – 61 (2010).
6. V. Karitans, M. Ozolinsh, L. Ekimane, K. Luse. „Dependence of Vernier acuity on the extent of retinal blur". Latvian Journal of Physics and Technical Sciences 48, 49 – 57 (2011).
7. K. Luse, A. Pausus, V. Karitans, M. Ozolins, M. Tukisa. „Evaluation of retro-reflective coating performance by reflectance and perceived relative brightness measurements". IOP Conf. Series: Materials Science and Engineering 23, 1 – 5 (2011).
8. V. Karitans, M. Ozolinsh, S. Fomins, A. Svede, G. Krumina, N. Iroshnikov. „Influence of ocular aberrations on the diameter of retinal blood vessels". Journal of Modern Optics 58, 1703 – 1709, 2011.
9. M. Ozolinsh, I. Martin, D. Lauva, V. Karitans „Howard-Dolman stereovision test at different opponent colour stimuli". Journal of Modern Optics 58, 1749 – 1754, 2011.
10. V. Karitans, M. Ozolinsh, L. Ekimane, K. Luse. „Presence of spherical aberration in the reference as a possible source of variations in magnitude of measured ocular aberrations". (accepted for publication in the journal 'Optica Applicata' and will be published in volume 42, issue 3).

List of conference abstracts

1. V. Karitans, M. Ozolinsh. "Perception of saturation ofcolours and dominant wavelength discrimination in central and peripheralretina." Eiropas Redzes Uztveres Konference ECVP-2007, Arezzo, Italy, 23.08.2007.-27.08.2007. Perception Supplement 36 p.193
2. M. Ozolinsh, V. Karitans. „Vai viegli ieskatīties pašam sev acīs?" Pirmais Latvijas inovatīvās mikroskopijas seminārs, Daugavpils, Latvija, 27.04.2007-29.04.2007.
3. V. Karitans, M. Ozolinsh. „Dynamical Visual Acquity in thePresence of Light Scattering." Photonics and Informatics, St. Petersburg, Russia, 04.09.2006. – 07.09.2006. Proceedings pp. 269-270.
4. V. Karitans, M. Ozolinsh, G. Kuprisha "Electronic eyeoccluder with time-counting and reflection control." 6th InternationalConference Advanced optical materials and devices, Riga, Latvia, 24.08.2008. – 27.08.2008. Programmeand Abstract p. 90.
5. V. Karitāns, M.Ozoliņš, S. Fomins, "Adaptīvā optika redzes zinātnei – hiperasuma pētījumi acīar koriģētām augstāko kārtu aberācijām." LU CFI. 25. zinātniskā konference,veltīta doc. Ludviga Jansona simtgadei, Rīga, Latvija, 11.02.2009. -13.02.2009. Tēžu grāmata 48. lpp.
6. V. Karitans, M. Ozolinsh, „Vernier acuity inpresence/absence of eye aberrations." Developments in Optics and Communications-2009, Riga, Latvia, 24.04.2009.-26.04.2009. Abstract book p.41.
7. V. Karitans, M. Ozolinsh, S. Fomins, „Dependence of Vernier acuity on the presence/ absence of aberrations of a human eye." Eiropas Redzes Uztveres Konference ECVP-2009, Regensburg, Germany, 24.08.2009.-28.08.2009. Perception Supplement 38 p.128
8. V. Karitans, M. Ozolinsh, „Methods of Compensating EyeMovements in Adaptive Optics Systems" Developments in Optics and Communications– 2010, Riga, Latvia, 23.04.2010. – 25.04.2010. Abstract book p. 35
9. V. Karitans, M. Kuibida, „Aberāciju ietekme uz dihoptiskuattēlu atšķiršanas spēju" Konference Lāzeram 50, Daugavpils, Latvija, 28.06.2010. – 29.06.2010. Tēžu grāmata p. 23
10. V. Karitans, M. Ozolinsh, „Simulating Retinal Vascular Disorders by Imposing Different Types of Higher-order Aberrations on RetinalImages". 5th European Meeting on Visual and Physiological Optics (EMVPO), Stockholm, Sweden, 22.08.2010. – 24.08.2010. Abstract book p.58.
11. V. Karitans, M. Ozolinsh, K. Luse. „Dependence of wavefront aberrations on spectral properties of Shack-Hartmann wavefront sensor". Functional Materials and Nanotechnologies – 2011, Riga, Latvia, 05.04.2011. – 08.04.2011. Abstract book p. 102.
12. K. Luse, A. Pausus, V. Karitans, M. Ozolins, M. Tukisa. „Evaluation of commercial retroreflective coating performance in decreased visibility conditions". Functional Materials and Nanotechnologies – 2011, Riga, Latvia, 05.04.2011. – 08.04.2011. Abstract book p. 100.
13. V. Karitans, M. Ozolinsh, S. Fomins, N. Iroshnikov, A. Larichev. „A/V Ratio as Predicted by Full Width at Half Maximumand by Blood Vessel Tracking in Presence of Ocular Aberrations". Adaptive Optics: Methods, Analysis, Applications, Toronto, Canada, 08.07.2011.– 14.07.2011. Abstract book p. 32.
14. V. Karitans, M. Ozolish. „Vernier acuity as a function of higher-order ocular aberrations". DOC-2011, Riga, Latvia, 28.04.2011. – 30.04.2011. Abstract book p. 68.
15. E. Skutele, V. Karitans. „Producing of ray tracing aberrometer for studying wavefront deformations". DOC-2011, Riga, Latvia, 28.04.2011. – 30.04.2011. Abstract book p. 70.
16. K. Luse, M. Ozolins, V. Karitans, I. Jekabsone. „Effect of position of retroreflective signs on recognition of pedestrian in reduced visibility conditions". DOC-2011, Riga, Latvia, 28.04.2011. – 30.04.2011. Abstract book p. 26.

Gratitude

The author wants to express grateful thanks to the supervisor of the doctoral work prof. **Maris Ozolins** for his support and intereset in my work. I am also thankful to the professor **Ivars Lacis** for his responsiveness and help. I would also like to say thanks to **Sergejs Fomins, Karlis Kundzins, Elina Laizane** and **Modris Logins** for valuable advices and practical help. Special thanks to the Department of Optometry and Vision Science, Faculty of Physics and Mathematics, University of Latvia and colleagues from Institute of Solid State Physics, University of Latvia for their support. Thanks also to all students who were enrolled in experiments. Invaluable thanks to my friends and family for moral support.

The work was supported by the European Social Fund project "Support of doctoral studies at the University of Latvia".

ESF EIROPAS SOCIĀLAIS FONDS

EIROPAS SAVIENĪBA

IEGULDĪJUMS TAVĀ NĀKOTNĒ

LATVIJAS UNIVERSITĀTE ANNO 1919

Latvijas Universitātes Cietvielu fizikas institūts